TECHNICAL MEMORANDUMS

NATIONAL ADVISORY COMMITTEE FOR AERONAUTICS

No. 1023

TWO-DIMENSIONAL POTENTIAL FLOW PAST AN ORDINARY THICK WING PROFILE

By F. Keune

Jahrbuch 1938 der Deutschen Luftfahrtforschung

Washington
July 1942

NATIONAL ADVISORY COMMITTEE FOR AERONAUTICS

TECHNICAL MEMORANDUM NO. 1023

TWO-DIMENSIONAL POTENTIAL FLOW PAST AN ORDINARY THICK WING PROFILE*

By F. Keune

SUMMARY

This report deals with the development of a method which gives a lucid and convenient solution of the flow conditions in the vicinity of a common, thick airfoil section wherein the thickness of the profile is taken into account. The method consists in making the airfoil the streamline in a parallel flow by disposing on its mean line certain source and vortex distributions the fields of which are superposed on the parallel flow. These distributions of singularities are secured for the generalized Kármán-Trefftz profile by means of conformal transformation from the flow about a circle. Five different distribution functions are afforded for the density of superposition, which combine in a specified manner to the necessary distributions of singularity and represent a generalized Kármán-Trefftz profile in parallel flow. For these profiles the speed for each of the five distributions is then computed independently of the angle of attack.

This substitution of a profile theoretically secured by singularities is then extended to include more general airfoil shapes, since a simple method permits a close approximation of any profile by a generalized Karman-Trefftz profile with known substitution of singularities. This approximation then affords the solution of the velocity field in the neighborhood of the general thick airfoil by a convenient method. For each of the five functions of the superposition density a speed diagram is plotted; the curves of constant speed parallel to the coordinate axes are combined to an orthogonal system. The readily discernible effects of the individual singularity distributions on the speed at any point of the plane of the section

*"Die ebene Potentialströmung um allgemeine dicke Tragflügelprofile." Jahrbuch 1938 der deutschen Luftfahrtforschung, pp. I 3 – I 26.

are in a simple manner correlated to the speeds. For comparison the speeds can be computed by the same method conformally to Birnbaum's approximation. It is found that the omission of the profile thickness is permissible only at great distances, that is, approximately of the order of magnitude of a wing chord.

A method is also given which affords a check on the agreement of the profile contour with the closed streamline defined by the singularity distributions. A further method enables the prediction of the profile contour for any selected singularity distribution.

After completion of this article, Z.f.a.M.M., vol. 18, 1938, p. 107, carried a report by F. Weinig, entitled: "The Flow Conditions in the Field of Thin, Slightly Cambered Airfoil Sections," which gives the velocity distributions for thin profiles in accord with the writer's calculations (figs. 26, 27, and 28). Weinig also considered the effects of complicated camber shapes. But the essential of the present article is the determination of the effect of profile thickness, which was not considered in Weinig's report; although it is very pronounced, according to present study. In general, it should be stronger than the effects of the mean-line forms exceeding Birnbaum's formulas.

INTRODUCTION

A solution of the two-dimensional flow about thin airfoil sections is afforded from either Birnbaum's method (reference 1) or Glauert's (reference 2) by the superposition of vortices on the mean line of the profile. But this theory fails to allow for the profile thickness. While the two-dimensional flow about thick profiles can be solved by means of conformal transformation, it involves considerable paper work, except for particular families, such as the Joukowski, Karman-Trefftz, and generalized Kármán-Trefftz airfoils (reference 3). In addition to that, these arguments do not lend themselves to the solution of the flow in vicinity of a wing of finite span, because conformal transformation is applicable only to two-dimensional flow and the application of the data derived from it to three-dimensional processes is limited to particularly favorable cases. On the other hand, these interference fields in three-dimensional flows are fre-

quently important, especially for biplane calculations.* Hence, if the thickness effect of a profile in all such calculations is to be accounted for, the conformal transformation must be abandoned in favor of the singularity method as for the thin profile.

The method of singularities consists in visualizing within the body in a stream another stream that forms the analytical continuation of the stream outside the body. The total flow has a closed streamline which coincides with the body contour. For the flow within the analytical continuation yields singularities, namely, sources and vortices. The total flow can be interpreted as the field of these singularities. Thus the plane flow about a cylinder is represented by a doublet superposition on a parallel flow (that is, the flow from a source to a sink located infinitely close to one another). The cylinder radius is defined by the ratio of doublet intensity to speed at infinity. If the cylinder has lift, a vortex flow past the cylinder axis must be added. In general, it requires several, usually continuously distributed singularities rather than singularities in a single point as in this instance. On surfaces of the type of airfoil sections the singularities are usually located along a line, that is, on the mean line. The displacement of the streamlines from the mean line corresponding to the finite thickness is effected by a source distribution; whereas a vortex distribution produces the lift-inducing deflection of flow. Such representation of flow past a profile is always possible if the flow in the outer space can be analytically continued on the inside (theory of analytical functions) so that the singular points of the function are disposed on a line wholly within the profile. This is necessary because it is conceivable that isolated singular points might yet be present; although they are likely to occur only along the chord by very radical thickness changes, such as are not apt to be encountered on the conventional airfoil shapes.

The principal task of the present report is to evolve a simple method by means of which the intensity and the position of the singularities can be so defined that the closed streamline resulting from the superposition of the singularity flow on the parallel flow is coincident with the given profile contour.

---

*The solution of this problem forms the subject of a special report.

If a symmetrical profile is chosen, the singularities will, for reasons of symmetry, be located on the mean line. Then the singularities could be determined in a similar manner as known from the calculation of the flow past airship hulls, by assuming the source distributions partly constant as proposed by Von Kármán (reference 4) and so defining the unknown intensities that the body contour becomes stream surface. But then the determination of the starting point of the superposition involves unusual difficulties. If it is wrongly chosen, the density of superposition at the start fluctuates between positive and negative values, which was the very reason for the ultimate change to surface superposition on airship hulls, especially in the case of transverse flow so as to avoid these difficulties (reference 5). For the two-dimensional problem in question a different line of attack is pursued from the very beginning. Since the flow past airfoils of a certain family is readily afforded from the flow past a circle by means of conformal transformation, the singularity substitute is forthwith computable for such profiles after inclusion of the flow within the conformal circle. Certain laws and typical distribution functions are acquired here which are faithfully transformed into general profile forms.

If the singularity distributions are given, the next problem consists in computing the flows of the separately found singularity distributions which are then easily combined into the desired flow of a prescribed profile.

With the computed singularity distributions new profile forms with desired form characteristics can also be constructed without having to resort to conformal transformation.

NOTATION

$\sigma = \omega + i\tau$	point in the plane of the circle
$\zeta = \xi + i\eta$	consecutive point in the plane of the section
$z = x + iy$	starting point in the plane of the section
$\bar{y} = y - y_s$	ordinate in the plane of the section measured from the mean line
y_s	ordinate of the mean line

y_Ψ ordinate of the streamline

y_1 ordinate of the mean line at point $x = +\frac{a'}{2}$

y_2 ordinate of the mean line at point $x = -\frac{a'}{2}$

D_1 thickness of profile at point $x = +\frac{a'}{2}$

D_2 thickness of profile at point $x = -\frac{a'}{2}$

D_{max} maximum thickness of profile

t profile chord

a distance $\overline{OA_1}$, criterion in plane of circle

a' half distance of branching points in plane of section

d measure for profile thickness

$\tan \beta$ measure for profile camber

μ measure for reversed curvature of profile

$\delta = \kappa\pi$ trailing edge angle of profile in radians

$\Phi(\sigma)$, $\Phi(z)$ complex potential function in plane of circle and section, respectively

$\Psi(\sigma)$, $\Psi(z)$ stream function in plane of circle and section, respectively

$V_\infty e^{-i\alpha'}$ air flow in plane of circle

$V_\infty e^{-i\alpha}$ air flow in plane of section

$V_x = V_\infty \cos \alpha$ component of flow in x direction

$V_y = V_\infty \sin \alpha$ component of flow in y direction

v_n normal component of velocity at the slit in plane ζ and z, respectively

v_t tangential component of velocity at the slit in plane ζ and z, respectively

u speed along x axis in plane of section

v speed along y axis in plane of section

w absolute amount of speed in plane of section

ϑ angle of speed toward positive x axis of plane of section

$q_\nu(\zeta)$, $q_\nu\left(\frac{\zeta}{a'}\right)$ strength of source per unit distance

$\gamma_\nu(\zeta)$, $\gamma_\nu\left(\frac{\zeta}{a'}\right)$ strength of vortex per unit distance

$f_\nu\left(\frac{\zeta}{a'}\right)$ base function of the singularity distributions with the ordinal number ν

$Q_\nu\left(\frac{x}{a'}; \frac{\bar{y}}{a'}\right)$ ratio of integral of flow function of source distribution $f_\nu\left(\frac{\zeta}{a'}\right)$ to undisturbed air flow at point $\frac{x}{a'}; \frac{\bar{y}}{a'}$

$W_\nu\left(\frac{x}{a'}; \frac{\bar{y}}{a'}\right)$ ratio of the integral of the flow function of the vortex distribution $f_\nu\left(\frac{\zeta}{a'}\right)$

I. THEORY

1. Solution of Singularities

a) Joukowski Profile

The Joukowski profile K_2' (fig. 1) in the ζ plane in the reflection of a circle K_2 in the σ plane, transformed by the conformal function

$$\zeta = \sigma + \frac{a^2}{\sigma} \tag{1}$$

frome plane σ in plane ζ. This circle K_2 is given by three quantities, namely, distance $\overline{A_1A_2} = 2a$, which defines the profile chord, distance $\overline{OO_1} = \alpha \tan \beta$, which defines the profile camber and distance $\overline{O_1O_2} = d$, which defines the profile thickness. From these quantities the radius of circle K_2 follows at

$$R = \frac{a}{\cos \beta} + d \tag{2}$$

its midpoint O_2 has the coordinates

$$\sigma_o = - d \cos \beta + i(a \tan \beta + d \sin \beta) \tag{3}$$

Circle K_1, with center O_1, and radius $\frac{a}{\cos \beta}$ and a radius vector amounting to

$$r \approx a \left(1 + \tan \beta \sin \varphi + \frac{1}{2} \tan^2 \beta \sin^2 \varphi\right) \tag{4}$$

(fig. 1) is transformed by the conformal function (1) in a double curve K_1', considered herein as the mean line of the profile. Its coordinates are:

$$\left.\begin{aligned} \frac{\xi}{2a} = \frac{\xi}{a'} &\approx \cos \varphi \left(1 + \frac{1}{2} \tan^2 \beta \sin^2 \varphi\right) \\ \frac{\eta}{2a} = \frac{\eta}{a'} &\approx \tan \beta \sin^2 \varphi \end{aligned}\right\} \tag{5}$$

or

$$\frac{\eta}{a'} \approx \tan \beta \left(1 - \frac{\xi^2}{a'^2}\right) \tag{6}$$

The slope of the mean line at any point $\frac{\xi}{a'}$ is accordingly

$$\frac{d\eta}{d\xi} = \tan \nu \approx -2 \tan \beta \cos \varphi \tag{7}$$

The inside of this circle K_1 then forms the second position of the ζ plane, so that the mean line K_1' is at the same time the slit in the original position for transition into the second. Points A_1' and A_2' are the branch points of the transformation. The distance of these points from the zero point is $\overline{O'A_1'} = \overline{O'A_2'} = 2a = a'$.

The flow past profile K_2' is obtained by transforming with function (1) the flow past circle K_2 from plane σ into plane ζ. This flow in plane σ, wherein circle K_2 is in a parallel flow at angle α' and speed V_∞ at infinity, is given by the complex flow potential

$$\Phi(\sigma) = V_\infty \left[(\sigma - \sigma_0) e^{-i\alpha'} + \frac{R^2 e^{i\alpha'}}{\sigma - \sigma_0}\right] + i \frac{\Gamma}{2\pi} \ln \frac{\sigma - \sigma_0}{R} \tag{8}$$

If, to insure smooth flow-off at the trailing edge, a stagnation point is to be located in point A_1, then it must be that

$$\Gamma = 4\pi V_\infty R \sin(\alpha' + \beta) \tag{9}$$

Now when the flow conditions within the profile are considered as continuation of the looked-for flow in the outer space, it is hardly to be expected that the same speeds prevail on the upper and lower edge of the assumedly double slit K_1', because these edges form the transition to the second position. This is readily apparent upon examination of the speeds at circle K_1 of plane σ the upper arc $A_1B_1A_2$ of which becomes the upper edge and the lower arc $A_2B_2A_1$ becomes the lower border of the slit. The flow past circle K_2 affords the speed at circle K_1; whereas conformal function (1) yields the speed at the slit which can be divided in its normal and tangential components. To get rid of the conformal transformation, the plane of the profile, plane ζ, must be interpreted as plane closed in itself, wherein the slit loses its significance and becomes the mean line. Then, however, the difference of the normal speeds v_n on the upper and lower border of the slit must be interpreted as source superposition (see fig. 2) and that of v_t as vortex superposition. The source strength q per unit length at a point ζ_1 of the mean line is accordingly given by

$$q(\zeta_1) = (v_{n_{ob}})_{\zeta_1} - (v_{n_u})_{\zeta_1} \tag{10}$$

and the vortex strength γ per unit length by

$$\gamma(\zeta_1) = (v_{t_{ob}})_{\zeta_1} - (v_{t_u})_{\zeta_1} \tag{11}$$

With these data the singularity distributions for a Joukowski profile can be computed.

For future purposes the flow velocity V_∞ in plane σ (fig. 1) is divided in its components parallel to the axes of the coordinates

$$\left.\begin{aligned} V_\omega &= V_\infty \cos \alpha' \\ V_\tau &= V_\infty \sin \alpha' \end{aligned}\right\} \tag{12}$$

and each of the flows created by the components is analyzed separately. The complex flow potential (8) divided conformally to (12) affords the speeds $\underline{v}_\sigma$ in the σ plane and the speeds $\underline{v}_\zeta = u - iv$ through the known relation $\underline{v}_\zeta = \underline{v}_\sigma \frac{d\sigma}{d\zeta}$. The speed in the ζ plane produced by the ω flow reads

$$\frac{d\,\Phi_\omega}{d\zeta} = \frac{d\,\Phi(\sigma)_\omega}{d\,\sigma}\,\frac{d\sigma}{d\zeta} =$$

$$V_\omega\,\frac{\dfrac{\sigma}{a} - \dfrac{R^2}{a^2}\left[\dfrac{a}{\sigma} + 2\dfrac{\sigma_o}{a}\dfrac{a^2}{\sigma^2} + 3\dfrac{\sigma_o^2}{a^2}\dfrac{a^3}{\sigma^3}\right] + 2i\dfrac{R}{a}\sin\beta\left[1 + \dfrac{\sigma_o}{a}\dfrac{a}{\sigma} + \dfrac{\sigma_o^2}{a^2}\dfrac{a^2}{\sigma^2}\right]}{\dfrac{\sigma}{a} - \dfrac{a}{\sigma}} \qquad (13)$$

and that due to the τ flow is:

$$\frac{d\,\Phi_\tau}{d\zeta} = \frac{d\,\Phi(\sigma)_\tau}{d\,\sigma}\,\frac{d\sigma}{d\zeta} =$$

$$-iV_\tau\,\frac{\dfrac{\sigma}{a} + \dfrac{R^2}{a^2}\left[\dfrac{a}{\sigma} + 2\dfrac{\sigma_o}{a}\dfrac{a^2}{\sigma^2} + 3\dfrac{\sigma_o^2}{a^2}\dfrac{a^3}{\sigma^3}\right] - 2\dfrac{R}{a}\cos\beta\left[1 + \dfrac{\sigma_o}{a}\dfrac{a}{\sigma} + \dfrac{\sigma_o^2}{a^2}\dfrac{a^2}{\sigma^2}\right]}{\dfrac{\sigma}{a} - \dfrac{a}{\sigma}} \qquad (14)$$

on the assumption that the distance $|\sigma_o|$ of the center O_2 of the circle from the zero point is short compared to a and hence small compared with $|\sigma| = r$. This is always the case when restricted to the conventional profiles where d/a is always $\ll 1$ and $\tan\beta \ll 1$; hence, especially thick strut sections are discounted.

Entering the values (2), (3), and (4) in equations (13) and (14), where $\sigma = r\,e^{i\varphi}$ indicates the coordinates of circle K_1, gives the velocities on the mean line, the real and imaginary part representing the components u and $(-v)$ along the coordinate axes. From these, with consideration to equation (7), the tangential and normal components follow at

$$\left.\begin{aligned} v_t &= u(1 - 2\tan^2\beta\cos^2\varphi) - 2v\tan\beta\cos\varphi \\ v_n &= 2u\tan\beta\cos\varphi + v(1 - 2\tan^2\beta\cos^2\varphi) \end{aligned}\right\} \qquad (15)$$

(see fig. 3).

After expansion of the speeds (equations (13) and (14)) in powers of d/a and $\tan\beta$ – the terms of higher than the second order are considered negligible – there is obtained with equation (15) and consideration of (10) and (11) a close approximation for the singularity distributions of the Joukowski profile.

For the flow along the ω axis the source distribution reads*

$$q(\varphi) = -2 V_\omega \frac{1}{\sin\varphi} \left\{ \frac{d}{a}[\cos\varphi(1-\cos\varphi) + \sin^2\varphi] \right|$$

$$+ 2\frac{d^2}{a^2}[\cos\varphi(1-\cos\varphi) + \sin^2\varphi - 3\sin^2\varphi\cos\varphi] + \ldots \Big\} \quad (16)$$

and for the vertex distribution

$$\gamma(\varphi) = 2 V_\omega \left\{ 2\tan\beta\sin\varphi \right| - \frac{d}{a}\tan\beta \left[\frac{1-\cos\varphi}{\sin\varphi} - 4\sin\varphi + 6\sin\varphi\cos\varphi \right] + \ldots \Big\} \quad (17)$$

and for the source distribution along the τ axis

$$q(\varphi) = \left| -6 V_\tau \frac{d}{a}\tan\beta \left[\frac{\cos\varphi(1-\cos\varphi)}{\sin\varphi} + \sin\varphi - 2\sin\varphi\cos\varphi \right] + \ldots \right. \quad (18)$$

and the vortex distribution

$$\gamma(\varphi) = 2 V_\tau \left\{ \frac{1-\cos\varphi}{\sin\varphi} + 2\frac{d}{a}\left[\frac{1-\cos\varphi}{\sin\varphi} - \sin\varphi \right] \right|$$

$$+ 3\frac{d^2}{a^2}\left[\frac{1-\cos\varphi}{\sin\varphi} - 2\sin\varphi + 2\sin\varphi\cos\varphi \right]$$

$$- \frac{d}{a}\tan\beta \left[\frac{1-\cos\varphi}{\sin\varphi} - 4\sin\varphi + 6\sin\varphi\cos\varphi \right]$$

$$- \tan^2\beta \left[\frac{1-\cos\varphi}{\sin\varphi} - \frac{1}{2}\sin\varphi + 2\sin\varphi\cos\varphi \right] + \ldots \Big\} \quad (19)$$

Between the angles φ of plane σ and the running coordinates of plane ζ the simple relation

---

*The heavy separation lines in the formulas indicate the places where the equations should be broken off when terms of the second degree are discounted.

$$\cos \varphi \approx \frac{\xi}{a'} \tag{20}$$

exists according to equation (5); besides, the flow at infinity remains unchanged in quantity and direction in the transformation, so that $V_\omega = V_x$, $V_T = V_y$, and $\alpha' = \alpha$.

A study of the computed singularity distributions discloses a consistent recurrence of the individual analytical expressions for the superposition density from which the entire distribution can be obtained. They are the four analytical expressions

$$\left.\begin{aligned}
f_1(\xi/a') &= \frac{1}{\sin \varphi}[\cos \varphi(1 - \cos \varphi) + \sin^2 \varphi] \\
&= + \sqrt{\frac{1 - \xi/a'}{1 + \xi/a'}}\,(1 + 2\,\xi/a') \\
f_2(\xi/a') &= \frac{1 - \cos \varphi}{\sin \varphi} = + \sqrt{\frac{1 - \xi/a'}{1 + \xi/a'}} \\
f_3(\xi/a') &= \sin \varphi = + \sqrt{1 - \left(\frac{\xi}{a'}\right)^2} \\
f_4(\xi/a') &= \sin \varphi \cos \varphi = \frac{\xi}{a'} \sqrt{1 - \left(\frac{\xi}{a'}\right)^2}
\end{aligned}\right\} \tag{21}$$

which, for practical reasons, are treated individually. The expression for the source distribution $f_1(\xi/a')$ is given separately; although it is composed of f_2 and f_3:

$$f_1(\xi/a') = 2f_3(\xi/a') - f_2(\xi/a') \tag{22}$$

because of the necessary secondary condition

$$\frac{1}{a'} \int_{-a'}^{+a'} f(\xi/a')\,d\xi = 0 \tag{23}$$

which must accompany all source distributions. Through it the contour stipulated by the source distribution $f\left(\frac{\xi}{a'}\right)$ becomes a closed curve at infinity. Functions $f_1\left(\frac{\xi}{a'}\right)$ and $f_4\left(\frac{\xi}{a'}\right)$ of which the source distributions (16) and (18) are composed, each satisfies this condition (23) by itself.

In the distributions $f_2\left(\frac{\xi}{a'}\right)$ and $f_3\left(\frac{\xi}{a'}\right)$ there can be recognized the well-known Birnbaum formulas (reference 1) for the vortex distributions which transform a flat or curved plate into a streamline. It affords, according to (19), the vortex distribution for the plate which is always occurring

$$\gamma_2\left(\frac{\xi}{a'}\right) = 2\ V_y \sqrt{\frac{1 - \xi/a'}{1 + \xi/a'}} = 2\ V_y f_2\left(\frac{\xi}{a'}\right) \tag{24}$$

and, according to (17), the vortex distribution which indicates the effect of the curvature and produces a rotation of the zero lift direction ($\alpha_0 = -\beta$):

$$\gamma_3\left(\frac{\xi}{a'}\right) = 4\ V_x \tan\beta \sqrt{1 - (\xi/a')^2} = 4\ V_x \tan\beta\ f_3\left(\frac{\xi}{a'}\right) \tag{25}$$

These known Birnbaum distributions are supplemented further by the effects due to profile thickness, that is, the source distribution (equation (16)):

$$q_1\left(\frac{\xi}{a'}\right) = -2\ V_x \frac{d}{a} \sqrt{\frac{1 - \xi/a'}{1 + \xi/a'}} \left(1 + 2\frac{\xi}{a'}\right) = -2\ V_x \frac{d}{a} f_1\left(\frac{\xi}{a'}\right) \tag{26}$$

and the vortex distribution (equation (19))

$$\gamma_{23}\left(\frac{\xi}{a'}\right) = -4\ V_y \frac{d}{a} \sqrt{\frac{1 - \xi/a'}{1 + \xi/a'}} \frac{\xi}{a'} = -4\ V_y \frac{d}{a}\left[f_3\left(\frac{\xi}{a'}\right) - f_2\left(\frac{\xi}{a'}\right)\right] \tag{27}$$

The quadratic terms are discounted for the present. They

merely afford in closest proximity of the profile contour a portion to the fow and are needed only when checking the coincidence of the closed streamline resulting from the singularities with the profile contour (cf. appendix). Otherwise they are important only for error appraisal.

All singularity distributions extend from $\xi = +a'$ to $\xi = -a'$, that is, from the trailing edge of the profile, the rear branch point A_1' to the forward branch point A_2', located slightly behind the nose. The distributions $f_1\left(\frac{\xi}{a'}\right)$ and $f_2\left(\frac{\xi}{a'}\right)$ have in the forward branching point $\xi = -a'$ an infinity point, that is, they approach infinity as $\left(1 + \frac{\xi}{a'}\right)^{-\frac{1}{2}}$.

b) The Kármán–Trefftz Profile

Whereas the Joukowski profiles terminate in an infinitely thin trailing edge, the Karman–Trefftz profiles form a finite angle δ on the trailing edge and so approach the commonly employed profiles much closer. Now the question arises as to the changes in the established distributions when a Kármán–Trefftz profile is to be streamline in a parallel flow. The conformal function

$$\frac{\zeta - ak}{\zeta + ak} = \left[\frac{\sigma - a}{\sigma + a}\right]^k \tag{28}$$

transforms the circle K_1 (fig. 4) in a crescent K_1' with angle δ, when

$$k = \frac{2\pi - \delta}{\pi} = 2 - \kappa \tag{29}$$

and

$$\kappa = \frac{\delta}{\pi} \tag{30}$$

For $\delta = 0$, circle K_1 becomes the infinitely thin mean line of the Joukowski profile, since (28) affords the conformal function (1). The Kármán–Trefftz profile will be, on the whole, thicker by the thickness of the crescent than the Joukowski profile. In view, therefore, of the singularity distributions a greater displacement flow may be anticipated, that is, a new source distribution; whereas the vortex distributions change very little. Our analysis will proceed therefore from a symmetrical Kármán–Trefftz profile.

On transformation of the σ plane in the ζ plane the upper or the lower rim of the crescent K_1' or any one curve in its interior becomes a slit in the ζ plane. The straight line $\overline{A_1'A_2'}$ is selected (fig. 4), that is, the median line K_3' of the crescent as slit, on the circumference of which the tangential and normal components of the speed must be computed as on the Joukowski profile. To this end the speeds in the σ plane on the reflection of this slit must be known, which follows from (28) at

$$\sigma = a\left[1 - \frac{\delta}{4}\left|\sin\psi\right|\left(1 + \frac{\kappa}{2} - \frac{\delta}{8}\left|\sin\psi\right|\right)\right]e^{i\psi} \qquad (31)$$

they are two circular arcs K_3 symmetrical to the ω axis, meeting in points A_1 and A_2 and having a radius vector of $|\sigma| \leqq a$, where ψ is the circular angle in the σ plane. After transformation the area bounded by the circular arcs K_3 forms the second position of the ζ plane.

For the speeds at the slit in the ζ plane equations (8) and (9) give the flow along the ω axis at:

$$\frac{d\Phi_\omega}{d\zeta} = \frac{d\Phi(\sigma)_\omega}{d\sigma}\frac{d\sigma}{d\zeta} = \frac{V_\omega}{k^2}\left[1 - \frac{R^2}{(\sigma - \sigma_0)^2}\right]\frac{1 - \frac{\sigma^2}{a^2}}{1 - \frac{\xi^2}{a'^2}} \qquad (32)$$

and the flow along the τ axis at:

$$\frac{d\Phi_\tau}{d\zeta} = \frac{d\Phi(\sigma)_\tau}{d\sigma}\frac{d\sigma}{d\zeta} = -i\frac{V_\tau}{k^2}\left[1 + \frac{R^2}{(\sigma - \sigma_0)^2} - 2R\frac{1}{\sigma - \sigma_0}\right]\frac{-1 - \frac{\sigma^2}{a^2}}{1 - \frac{\xi^2}{a'^2}} \qquad (33)$$

if $\tan\beta = 0$, $\sigma_0 = -d$, R is given by (2) and σ by (31). According to (10), the source distribution for the flow along the ξ axis follows from equation (32) at:

$$q\left(\frac{\xi}{a'}\right) = -\frac{8}{k^2}V_x\frac{\sin\psi}{1 - \frac{\xi^2}{a'^2}}\left\{\frac{d}{a}\left[\cos\psi\,(1 - \cos\psi) + \sin^2\psi\right]\right.$$

$$+ \frac{d}{2}\delta\left|\sin\psi\right|\cos\psi + 2\frac{d^2}{a^2}\left[\cos\psi\,(1 - \cos\psi)\right.$$

$$\left.\left. + \sin^2\psi - 3\sin^2\psi\cos\psi\right] + \frac{1}{4}\kappa\,\delta\left|\sin\psi\right|\cos\psi + \ldots\right\} \qquad (34)$$

and, according to equation (11), the vortex distribution of the same flow direction

$$\gamma\left(\frac{\xi}{a'}\right) = 0 \tag{34a}$$

For the flow along the η axis, equation (33) gives the source distribution

$$q\left(\frac{\xi}{a'}\right) = 0 \tag{35}$$

and the vortex distribution

$$\gamma\left(\frac{\xi}{a'}\right) = \frac{8}{k^2} V_y \frac{\sin\psi}{1 - \frac{\xi^2}{a'^2}} \left\{(1 - \cos\psi) + 2\frac{d}{a}\left[1 - \cos\psi - \sin^2\psi\right]\right.$$

$$+ 3\frac{d^2}{a^2}\left[1 - \cos\psi - 2\sin^2\psi + 2\sin^2\psi\cos\psi\right]$$

$$+ 2\frac{d}{a}\frac{\delta}{2}\left|\sin\psi\right|\left[1 - \cos\psi - \frac{3}{2}\sin^2\psi\right]$$

$$\left. + \frac{\delta^2}{32}\sin^2\psi(1 - 4\cos\psi) + \ldots\ldots\right\} \tag{36}$$

The transformation leaves the air flow at infinity unchanged. The secured singularity distributions also contain the circular angle ψ which is not as simply related to the abscissa ξ of ζ plane as the angle φ in the Joukowski transformation. In this instance the relation is obtained by entering the coordinates of circle K_3 (equation (31)) in the conformal function (28); then

$$\psi \approx 2\,(\tan^{-1})\left[\frac{1 - \frac{\xi}{a'}}{1 + \frac{\xi}{a'}}\right]^{1/k}\left[1 - \frac{1}{4}\frac{\delta^2}{16}\frac{\xi}{a'}\right] \tag{37}$$

For Joukowski profiles $\delta = 0$ and $k = 2$, then

$$\varphi \approx 2 \left(\tan^{-1}\right) \sqrt{\frac{1 - \frac{\xi}{a'}}{1 + \frac{\xi}{a'}}}, \quad \frac{\xi}{a'} \approx \cos \varphi \tag{38}$$

For practical reasons the coordinate $\frac{\xi}{a'}$ in the plane of the profile is now considered as a fixed given quantity, and ψ, related to $\frac{\xi}{a'}$ and δ through equation (37), is represented in the form

$$\psi \approx \varphi + \epsilon \tag{39}$$

The circular angle φ for Joukowski profiles is given by equation (38); angle ϵ is largely dependent on angle δ, specifically $\epsilon = 0$ for $\delta = 0$. With (39), equations (37) and (38) give

$$\epsilon\left(\frac{\xi}{a'}\right) \approx 2 \left(\tan^{-1}\right) \frac{\sqrt{\frac{1 - \xi/a'}{1 + \xi/a'}} \left\{ \left[\frac{1 - \xi/a'}{1 + \xi/a'}\right]^{\kappa/4} - 1 \right\}}{1 + \left[\frac{1 - \xi/a'}{1 + \xi/a'}\right]\left[\frac{1 - \xi/a'}{1 + \xi/a'}\right]^{\kappa/4}} \tag{40}$$

and $\epsilon(-\xi/a') = -\epsilon(+\xi/a')$. The correction angle $\epsilon\left(\frac{\xi}{a'}\right)$ is small for the usual δ and in close approximation may be considered linear in δ and κ, respectively, as exemplified in figure 5, where $\frac{\epsilon(\xi/a')}{\kappa}$ is plotted against $\frac{\xi}{a'}$ independently of κ.

Expression (36) then affords with (38) and (39) the analytical expressions for the superposition density

$$\left.\begin{aligned}
\bar{f}_1\left(\frac{\xi}{a'}\right) &= \frac{\sin\psi}{1-\frac{\xi^2}{a'^2}}\cdot\left\{\cos\psi(1-\cos\psi)+\sin^2\psi\right\} \\
&= f_1\left(\frac{\xi}{a'}\right)\Big| + \epsilon\left(\frac{\xi}{a'}\right)\left[4\,\frac{\xi}{a'}-\frac{1-2\frac{\xi^2}{a'^2}}{1+\xi/a'}\right] \\
\bar{f}_2\left(\frac{\xi}{a'}\right) &= \frac{\sin\psi}{1-\frac{\xi^2}{a'^2}}\,(1-\cos\psi) = f_2\left(\frac{\xi}{a'}\right)\Big| + \epsilon\left(\frac{\xi}{a'}\right)\frac{1+2\xi/a'}{1+\xi/a'} \\
\bar{f}_4\left(\frac{\xi}{a'}\right) &= \frac{\sin^3\psi}{1-\frac{\xi^2}{a'^2}}\cos\psi = f_4\left(\frac{\xi}{a'}\right)\Big| - \epsilon\left(\frac{\xi}{a'}\right)\left(1-\frac{\xi^2}{a'^2}\right)
\end{aligned}\right\} \quad (41)$$

differing only by an additive term from the original expression (21). They also have zero or infinity places at the branch point A_2' just as the expressions $f_\nu(\xi/a')$, except that the limiting values at these places $\xi/a' = \pm 1$ are now reached with the power* $(1-\xi/a')^{-\frac{1}{2}\left[1-\frac{\kappa}{2}\right]}$. However, even this change in the singularity functions included in the correction term is negligibly small for all usual angles ($\delta \leqq 36^\circ$).

These known expressions are supplemented by a new one for the singularity distributions of the crescent:

$$\bar{f}_5\left(\frac{\xi}{a'}\right) = \frac{\sin\psi}{1-\frac{\xi^2}{a'^2}}\,|\sin\psi|\cos\psi = f_5\left(\frac{\xi}{a'}\right) - \epsilon\left(\frac{\xi}{a'}\right)\frac{1-3\frac{\xi^2}{a'^2}}{\sqrt{1-\frac{\xi^2}{a'^2}}} \quad (42)$$

*If $\xi = -(a'-\Delta)$, equation (40) becomes

$$\epsilon\left[-(a'-\Delta)\right] = +2\left[\frac{\Delta}{2a'}\right]^{1/2}\left\{1-\left[\frac{\Delta}{2a'}\right]^{\kappa/4}+\ldots\right\}$$

where $$f_5\left(\frac{\xi}{a'}\right) = \cos\varphi = \frac{\xi}{a'} \tag{42a}$$

Function $\bar{f}_5\left(\frac{\xi}{a'}\right)$ gives the source distribution of the crescent

$$\bar{q}_5\left(\frac{\xi}{a'}\right) = -\delta\bar{f}_5\left(\frac{\xi}{a'}\right). \tag{43}$$

For the singularity distributions of the Kármán-Trefftz profiles, the factor $\frac{4}{k^2} = 1 + \kappa + \ldots$ is supplementary to those of the Joukowski profile; it affords, besides the vortex distribution caused by the thickness of the crescent,

$$\gamma_2'\left(\frac{\xi}{a'}\right) = \kappa\,\gamma_2\left(\frac{\xi}{a'}\right) \tag{44}$$

merely distributions which are small from the second degree at least. Summed up, there is obtained, besides the Joukowski profile singularity distributions, additional distributions for the symmetrical Kármán-Trefftz profiles: namely, the source distribution $\bar{q}_5(\xi/a')$ and the vortex distribution $\kappa\gamma_2(\xi/a')$, which, taken by themselves, represent a crescent. For curved Kármán-Trefftz profiles the afore-mentioned terms are supplemented by others which are dependent upon edge angle and camber. But an exact calculation discloses all these terms to be small, at least from the second degree.

c) Profiles with Reversed Curvature (S profiles)

The mean line of both the Joukowski and the Kármán-Trefftz profiles is a circular arc. But the form of the mean line of a general profile usually differs from a circular arc for reasons of lesser center of pressure travel by angle-of-attack changes. This is achieved by an S-shaped mean line. The deformation of the circular-arclike mean line requires an additional vortex distribution on substitution of the profiles by singularities.

According to Betz and Keune (reference 3) a circle K_2 (fig. 4) is transformed into a profile with finite angle at the trailing edge and with reversed curvature by means of conformal function

$$\frac{\zeta - a'}{\zeta + a'} = \left[\frac{\sigma - a}{\sigma + a}\right]^k e^{i\mu\frac{a}{\sigma}} \qquad (45)$$

To secure the additive vortex distribution a circle K_1 is merely transformed into an infinitely thin S-shaped mean line (fig. 6) (that is, put $\delta = 0$, $k = 2$), because the different singularity distributions are known to be additive in first approximation. Furthermore, the criterion μ for the size of the reversed curvature is presumed to be small, so that terms which are quadratic in μ are negligibly small.

Development of the conformal function for small μ and $k = 2$ affords

$$\frac{\zeta}{a'} = \frac{1}{2a}\left\{\sigma + \frac{a^2}{\sigma} + i\,a\,\frac{\mu}{4}\,\frac{\sigma}{a}\left(1 - \frac{a^2}{\sigma^2}\right)^2\right\} \qquad (46)$$

It splits in the known Joukowski transformation and an additional conformal function.

The reflection of circle K_1 around 0 (fig. 6), $\sigma = a\,e^{i\varphi}$, is the slit, the mean line the ζ plane with the coordinates

$$\frac{\xi}{a'} = \cos\varphi - \frac{\mu}{2}\sin^3\varphi;\quad \frac{\eta}{a'} = -\frac{\mu}{2}\sin^2\varphi\cos\varphi$$

Hence

$$\frac{\eta}{a'} = -\frac{\mu}{2}\,\frac{\xi}{a'}\left(1 - \frac{\xi^2}{a'^2}\right) \qquad (47)$$

is the equation of the S-shaped mean line and

$$\tan\nu = \frac{d\,\eta}{d\,\xi} = -\frac{\mu}{2}\left(1 - 3\,\frac{\xi^2}{a'^2}\right) \qquad (48)$$

the direction of the tangents of the mean line to the ξ axis. Then the tangential and normal components of the velocities at the slit follow at

$$\left.\begin{aligned} v_t &= u - \frac{\mu}{2}\,(1 - 3\cos^2\varphi)\,v \\ v_n &= \frac{\mu}{2}\,(1 - 3\cos^2\varphi)\,u + v \end{aligned}\right\} \tag{49}$$

and equations (8) and (9) finally afford with (10) and (11) the vortex distributions for the S-shaped mean line:

$$\left.\begin{aligned} \gamma\left(\frac{\xi}{a'}\right) &= -\left[V_x + \frac{\mu}{4}\,V_y\right] 3\,\mu\,\sin\varphi\,\cos\varphi \\ \text{and} \\ \gamma\left(\frac{\xi}{a'}\right) &= 2\left[V_y - \frac{\mu}{4}\,V_x\right]\frac{1-\cos\varphi}{\sin\varphi} \end{aligned}\right\} \tag{50}$$

In these equations (50) the fact that the conformal functions (45) and (46), respectively, changes the air-flow direction at infinity has been borne in mind, giving

$$\left.\begin{aligned} V_\infty\cos\alpha' = V_w &= V_\infty\cos\left(\alpha - \frac{\mu}{4}\right) \approx V_x + \frac{\mu}{4}\,V_y \\ V_\infty\sin\alpha' = V_\tau &= V_\infty\sin\left(\alpha - \frac{\mu}{4}\right) \approx V_y - \frac{\mu}{4}\,V_x \end{aligned}\right\} \tag{51}$$

this change being interpreted as a rotation of the coordinate axes in the ζ plane.

Then the introduction of the analytical expressions (21) and the limitation to terms of the first rank affords, besides the known distribution for the plate.

$$\gamma_2\left(\frac{\xi}{a'}\right) = 2\,V_y\,f_2\left(\frac{\xi}{a'}\right)$$

the vortex distribution for the reversed curvature

$$\gamma_4\left(\frac{\xi}{a'}\right) = -3\,\mu\,V_x\sin\varphi\cos\varphi - \frac{\mu}{2}\,V_x\,\frac{1-\cos\varphi}{\sin\varphi}$$

$$= -3\,\mu\,V_x\left[f_4\left(\frac{\xi}{a'}\right) + \frac{1}{6}\,f_2\left(\frac{\xi}{a'}\right)\right] \tag{52}$$

the first part of which was given by Birnbaum (reference 1); while the second part is due to the rotation of the axes in flow direction.

The singularity distributions thus secured for a profile with finite edge angle and reversed curvature in first approximation, then, merely need to be combined in a certain manner to afford the field of flow of this profile.

If the vortex distribution of a selected mean line is to be established, it can be visualized approximately by the sum of circular arc (equation (6)) and reverse curvature (equation (47)). The coordinates of this approximation can be written in the form

$$\frac{\eta}{a'} = \left(\tan \beta - \frac{\mu}{2} \frac{\xi}{a'} \right) \left(1 - \frac{\xi^2}{a'^2} \right) \tag{53}$$

Then the directions of the tangents with the ξ axis are given by

$$\tan \nu = \frac{d\eta}{d\xi} = - 2 \frac{\xi}{a'} \tan \beta - \frac{\mu}{2} \left(1 - 3 \frac{\xi^2}{a'^2} \right) \tag{53a}$$

and with it the tangent in point $A_1'(\xi = +a')$ by $\tan \nu_1 = - 2 \tan \beta + \mu$ and the tangent in point $A_2' = (\xi = -a')$ by $\tan \nu_2 = 2 \tan \beta + \mu$.

The procedure in solving the profile constants $\tan \beta$ and μ can therefore be the same as Birnbaum's (reference 1), who derived them from the tangents at points A_1' and A_2'. But, since the tangents are hard to establish accurately at these points, it is more practical to define the curve of the third degree of the mean line from the ordinates. With η_1 denoting the ordinate at $\xi = + \frac{a'}{2}$ and η_2 the ordinate at $\xi = - \frac{a'}{2}$ (fig. 14), equation (53) gives

$$\left.\begin{aligned} \tan \beta &= \frac{2}{3} \left(\frac{\eta_2}{a'} + \frac{\eta_1}{a'} \right) \\ \mu &= \frac{8}{3} \left(\frac{\eta_2}{a'} - \frac{\eta_1}{a'} \right) \end{aligned}\right\} \tag{54}$$

This defines the profile constants for the case where the mean line is a curve of the third degree. Whether it is represented accurately enough by this curve can be checked by the degree of accuracy with which the ordinate value for $\xi = 0$ satisfies the condition $\eta_0/a' = \tan\beta$.

2. Flow in Plane of Section

a) Substitution of Profile by Singularities

The flow past a profile in parallel flow can be achieved by a certain continuous distribution of sources and vortices on the mean line of this profile. The flow produced by these singularities must be superposed on the parallel flow so that the closed streamline formed by these two flows agrees with the profile contour. The form of these singularity distributions was secured in the preceding chapter for profiles of certain families. If these distributions are to be used for the substitution of other profiles, the extent of the coincidence of the closed streamline with the contour must be checked. And this introduces the stream functions of the distributions.

The complex flow potential of a source element $q(\xi)\,ds$ in a point z is given by

$$\Phi_1(z) = \frac{q(\xi)}{2\pi}\ln(z-\zeta)\,ds$$

and for a vortex element $\gamma(\xi)\,ds$ by

$$\Phi_2(z) = \frac{i\,\gamma(\xi)}{2\pi}\ln(z-\zeta)\,ds$$

where ζ is the locus of the element (fig. 7). Integration with respect to all singularity elements along the arc length S of the mean line affords for the profile in parallel flow the stream function

$$\Phi(z) = V_\infty z e^{-i\alpha} + \frac{1}{2\pi}\int_S q(\xi)\ln(z-\zeta)\,ds + \frac{i}{2\pi}\int_S \gamma(\xi)\ln(z-\zeta)\,ds, \quad (55)$$

with V_∞ denoting the flow velocity and α the angle of attack respecting the positive x axis. The integral equation for the stream function

$$\Psi(z) = y V_\infty\cos\alpha - x V_\infty\sin\alpha + \frac{1}{2\pi}\int_S q(\xi)\operatorname{arc\,tg}\frac{y-\eta}{x-\xi}\,ds + \frac{1}{2\pi}\int_S \gamma(\xi)\ln\sqrt{(x-\xi)^2+(y-\eta)^2}\,ds, \quad (55a)$$

is now simplified so that the integrals can be numerically evaluated independently of the form of the mean line. Next, we introduce (fig. 8)

$$y = y_s + \bar{y}$$

whereby y_s, the ordinate of the mean line, can, according to (53), be written in form

$$\frac{y_s}{a'} \approx \left(\operatorname{tg}\beta - \frac{\mu}{2}\frac{x}{a'}\right)\left(1-\frac{x^2}{a'^2}\right)$$

Likewise

$$\frac{\eta}{a'} \approx \left(\operatorname{tg}\beta - \frac{\mu}{2}\frac{\xi}{a'}\right)\left(1-\frac{\xi^2}{a'^2}\right)$$

and the arc element ds itself is given according to (53a) by

$$ds = d\xi\sqrt{1+\left(\frac{d\eta}{d\xi}\right)^2} \approx d\xi$$

the small quadratic terms being discounted.

Herewith the integrals become

$$\int_S \gamma(\xi)\ln\sqrt{(x-\xi)^2+(y-\eta)^2}\,ds \approx \int_{-a'}^{+a'} \gamma(\xi)\ln\sqrt{(x-\xi)^2+\bar{y}^2}\,d\xi - \frac{\bar{y}}{a'}\operatorname{tg}\beta\int_{-a'}^{+a'}\gamma(\xi)\frac{(x-\xi)(x+\xi)}{(x-\xi)^2+\bar{y}^2}\,d\xi$$

$$+\frac{\bar{y}}{a'}\frac{\mu}{2}\int_{-a'}^{+a'}\gamma(\xi)\frac{\frac{\xi}{a'}(x-\xi)(x+\xi)}{(x-\xi)^2+\bar{y}^2}d\xi \quad \ldots \quad (56a)$$

and

$$\int_S q(\xi)\operatorname{arc\,tg}\frac{y-\eta}{x-\xi}ds \approx \underline{\int_{-a'}^{+a'} q(\xi)\operatorname{arc\,tg}\frac{\bar{y}}{x-\xi}d\xi}$$

$$-\frac{1}{a'}\operatorname{tg}\beta\int_{-a'}^{+a'}q(\xi)\frac{(x-\xi)^2(x+\xi)}{(x-\xi)^2+\bar{y}^2}d\xi$$

$$+\frac{1}{a'}\frac{\mu}{2}\int_{-a'}^{+a'}q(\xi)\frac{\frac{\xi}{a'}(x-\xi)^2\cdot(x+\xi)}{(x-\xi)^2+\bar{y}^2}d\xi \quad \ldots \quad (56b)$$

In addition to the underscored integrals independent of the form of the mean line, we obtain cumulative integrals multiplied by consistently small values $\tan\beta$ and μ and, together with the singularity distributions, they are therefore small, at least of the second degree. Hence, they have no further significance. We therefore dispose, similarly to Birnbaum (reference 1) and Glauert (reference 2), the singularities on the chord of the mean line, and so obtain

$$\Psi(z) = y V_\infty\cos\alpha - x V_\infty\sin\alpha + \frac{1}{2\pi}\int_{-a'}^{+a'}q(\xi)\operatorname{arc\,tg}\frac{\bar{y}}{x-\xi}d\xi +$$

$$+\frac{1}{2\pi}\int_{-a'}^{+a'}\gamma(\xi)\ln\sqrt{(x-\xi)^2+\bar{y}^2}\,d\xi. \quad (57)$$

for the stream function.

According to the foregoing, the singularities extend from A_1' to A_2'. Putting Ψ = const affords an integral equation indicating the field of all streamlines in the plane of the section, one of which is the closed streamline, that must agree with the section contour. Since all streamlines are defined merely up to one constant it is decided that this streamline shall obtain the value $\Psi = 0$. Then the streamline of the parallel flow which goes in the forward stagnation point of the section must, of course, carry the same identification. But, since this stagnation point is not generally known, some other method must be applied. The flow is therefore divided again into its components along the axes of the coordinates and the constants are so defined that, for the flow in the x direction, the rear stagnation A_1' and for the flow in the y direction, the profile point on the y axis ($x = 0$, $\bar{y} = \bar{y}_1$) lies on the streamline $\Psi = 0$. Then stream function (57) gives

$$\frac{\Psi_x}{a'V_x} = \frac{y}{a'} + \frac{d}{a}Q_1\left(\frac{x}{a'};\frac{\bar{y}}{a'}\right) + \frac{1}{2}\delta\bar{Q}_1\left(\frac{x}{a'};\frac{\bar{y}}{a'}\right)$$

$$+2\operatorname{tg}\beta\left[W_3\left(\frac{x}{a'};\frac{\bar{y}}{a'}\right)-W_3(1;0)\right]$$

$$-\frac{\mu}{4}\left\{\left[W_2\left(\frac{x}{a'};\frac{\bar{y}}{a'}\right)-W_2(1;0)\right]\right.$$

$$\left.+6\left[W_4\left(\frac{x}{a'};\frac{\bar{y}}{a'}\right)-W_4(1;0)\right]\right\}+g_x, \quad \ldots \quad (58)$$

for the flow along the x axis* and

$$-\frac{\Psi_y}{a'V_y} = \frac{x}{a'} - \left(1+2\frac{d}{a}+\varkappa\right)\left[W_2\frac{x}{a'};\frac{\bar{y}}{a'}\right)-W_2\left(0;\frac{\bar{y}_1}{a'}\right)\Big]$$

$$+2\frac{d}{a}\left[W_3\left(\frac{x}{a'};\frac{\bar{y}}{a'}\right)-W_3\left(0;\frac{\bar{y}_1}{a'}\right)\right]-g_y, \quad (59)$$

for the flow along the y axis, with abbreviation

$$-\frac{1}{\pi a'}\int_{-a'}^{+a'}f_\nu\left(\frac{\xi}{a'}\right)\operatorname{arc\,tg}\frac{\bar{y}}{x-\xi}d\xi$$

$$=\frac{1}{\pi a'}\int_{-a'}^{+a'}f_\nu\left(\frac{\xi}{a'}\right)\operatorname{arc\,tg}\frac{x-\xi}{\bar{y}}a_\nu = Q_\nu\left(\frac{x}{a'};\frac{\bar{y}}{a'}\right) \quad (60)$$

for the source-sink integrals** and

---

*The $-$ denotes the correction, according to formula (42).

**Formula (60) is evolved from the relation

$$+(\tan^{-1})\frac{\bar{y}}{x-\xi} = \pi - (\tan^{-1})\frac{x-\xi}{\bar{y}}$$

whereby, because of (23)

$$\frac{1}{\pi a'}\int_{-a'}^{+a'}\pi f_\nu\left(\frac{\xi}{a'}\right)d\xi = 0.$$

$$\frac{1}{\pi a'}\int_{-a'}^{+a'} f_\nu\left(\frac{\xi}{a'}\right)\ln\sqrt{\left(\frac{x}{a'}-\frac{\xi}{a'}\right)^2+\frac{\overline{y}^2}{a'^2}}\,d\xi = W_\nu\left(\frac{x}{a'};\frac{\overline{y}}{a'}\right) \quad (61)$$

for the vortex integrals, and g_x and g_y denoting the quadratic small terms. For the profile itself, we get $\bar{\Psi}_x = 0$ $\bar{\Psi}_y = 0$

$$\Psi = \Psi_x + \Psi_y \quad \ldots\ldots\ldots (62)$$

If the four constants $\frac{d}{a}$, δ, $\tan\beta$, and μ are correctly defined the contour of generalized Kármán-Trefftz profile (reference 3) should agree approximately with the streamline from equations (58) and (59), if necessary with allowance for the quadratic terms. The agreement can be checked numerically by means of the appended graphs which give the values of the flow function for the source distributions Q_ν (equation (60)) and for vortex distributions W_ν (equation (61)) plotted against the ordinate $\frac{\overline{y}}{a'}$ for various abscissas $\frac{x}{a'}$.

b) Field of Velocity in the Vicinity of a Profile

As a consequence of the resolution of the singularity distributions which transform a profile to a streamline in a parallel flow, the velocity field around this section is established without difficulty. The components of the speed are given by

$$\frac{\partial\Psi_{(z)}}{\partial y} = u;\quad \frac{\partial\Psi_{(z)}}{\partial x} = -v$$

and, according to (62),

$$\left.\begin{aligned} u &= \frac{\partial\Psi_x}{\partial y}+\frac{\partial\Psi_y}{\partial y}\\ -v &= \frac{\partial\Psi_x}{\partial x}+\frac{\partial\Psi_y}{\partial x}\end{aligned}\right\} \quad \ldots\ldots (63)$$

In this case also the effect of each singularity distribution is given separately, in order to preserve the lucid aspect of the effect of the individual profile constants.

Partial integration of (58) and (59) gives the four integrals

$$\left.\begin{aligned}
\frac{\partial Q_\nu}{\partial y/a'} &= -\frac{1}{\pi}\int_{-a'}^{+a'} f_\nu\left(\frac{\xi}{a'}\right)\frac{x-\xi}{(x-\xi)^2+\overline{y}^2}\,d\xi\\
&= -\frac{1}{\pi}\left\{\frac{x}{a'}P_1\left[f_\nu\left(\frac{\xi}{a'}\right)\right]-P_2\left[f_\nu\left(\frac{\xi}{a'}\right)\right]\right\}\\
\frac{\partial Q_\nu}{\partial x/a'} &= \frac{1}{\pi}\int_{-a'}^{+a'} f_\nu\left(\frac{\xi}{a'}\right)\frac{\overline{y}}{(x-\xi)^2+\overline{y}^2}\,d\xi\\
&= \frac{\overline{y}}{a'\pi}P_1\left[f_\nu\left(\frac{\xi}{a'}\right)\right]\\
\frac{\partial W_\nu}{\partial y/a'} &= \frac{1}{\pi}\int_{-a'}^{+a'} f_\nu\left(\frac{\xi}{a'}\right)\frac{\overline{y}}{(x-\xi)^2+\overline{y}^2}\,d\xi\\
&= \frac{\overline{y}}{a'\pi}P_1\left[f_\nu\left(\frac{\xi}{a'}\right)\right]
\end{aligned}\right\} \quad (64)$$

and

$$\left.\begin{aligned}
\frac{\partial W_\nu}{\partial x/a'} &= \frac{1}{\pi}\int_{-a'}^{+a'} f_\nu\left(\frac{\xi}{a'}\right)\frac{x-\xi}{(x-\xi)^2+\overline{y}^2}\,d\xi\\
&= \frac{1}{\pi}\left\{\frac{x}{a'}P_1\left[f_\nu\left(\frac{\xi}{a'}\right)\right]-P_2\left[f_\nu\left(\frac{\xi}{a'}\right)\right]\right\}
\end{aligned}\right\}$$

which divide into the two integrals

$$\left.\begin{aligned}
P_1\left[f_\nu\left(\frac{\xi}{a'}\right)\right] &= a'\int_{-a'}^{+a'} f_\nu\left(\frac{\xi}{a'}\right)\frac{d\xi}{(x-\xi)^2+\overline{y}^2}\\
\text{and}\qquad P_2\left[f_\nu\left(\frac{\xi}{a'}\right)\right] &= \int_{-a'}^{+a'} f_\nu\left(\frac{\xi}{a'}\right)\frac{\xi\,d\xi}{(x-\xi)^2+\overline{y}^2}
\end{aligned}\right\} \quad (65)$$

The singularity distributions $f_\nu\left(\frac{\xi}{a'}\right)$ can be written in the form

$$F\left(\frac{\xi}{a'}\right) = \sqrt{\frac{a'-\xi}{a'+\xi}}\left[C_1+C_2\frac{\xi}{a'}+C_3\frac{\xi^2}{a'^2}\right]$$

Therefore the resolution of the one general integral

$$J_n = \left(\frac{1}{a'}\right)^{n-1} \int_{-a'}^{+a'} \sqrt{\frac{a'-\xi}{a'+\xi}} \frac{\xi^n\, d\xi}{(x-\xi)^2+\bar{y}^2}$$

$$= \left(\frac{1}{a'}\right)^{n-1} \int_{-a'}^{+a'} \frac{(a'-\xi)\,\xi^n}{(x-\xi)^2+\bar{y}^2} \frac{d\xi}{\sqrt{a'^2-\xi^2}}, \quad \ldots \quad (66)$$

is sufficient, if n is a whole positive digit (n = 0, 1, 2, 3). After the substitution $\xi - x = w$,

$$(a')^{n-1} J = \int_{-(a'+x)}^{a'-x} \frac{[a'-x-w]\,[x+w]^n}{w^2+\bar{y}^2} \frac{dw}{\sqrt{a'^2-(w+x)^2}}.$$

Development of the integrand of this integral for $n \leq 3$ in powers of w gives the integral in the form

$$(a')^{n-1} J = b_1 L_1 + b_2 L_2 + b_3 L_3 + L_4 \quad \ldots \quad (67)$$

where

$$\left.\begin{aligned} L_1 &= \int_{-(a'+x)}^{a'-x} \frac{dw}{\sqrt{a'^2-(x+w)^2}} = +\pi \\ L_2 &= \int_{-(a'+x)}^{a'-x} \frac{w\,dw}{\sqrt{a'^2-(x+w)^2}} = -x\pi \end{aligned}\right\} \quad (68)$$

and

$$L_3 = \int_{-(a'+x)}^{a'-x} \frac{w^2\,dw}{\sqrt{a'^2-(x+w)^2}} = +\left(\frac{a'^2}{2}+x^2\right)\pi$$

while the solution of integral L_4 leads to

$$L_4 = \int_{-(a'+x)}^{a'-x} \frac{b_4 w + b_5}{w^2+\bar{y}^2} \frac{dw}{\sqrt{a'^2-(x+w)^2}} = \frac{b_4}{a'}\pi\Omega_1 - \frac{b_5}{a'^2}\pi\Omega_2 \quad (69)$$

where

$$\left.\begin{aligned} \Omega_1 &= \frac{\pm\sqrt{\frac{1}{2}\left[\lambda-\left(1-\frac{x^2}{a'^2}+\frac{\bar{y}^2}{a'^2}\right)\right]}}{\lambda} \\ \Omega_2 &= \frac{\frac{x}{a'}}{\pm\lambda\sqrt{\frac{1}{2}\left[\lambda-\left(1-\frac{x^2}{a'^2}+\frac{\bar{y}^2}{a'^2}\right)\right]}} \end{aligned}\right\} \quad \ldots \quad (70)$$

and

$$\lambda = +\sqrt{\left[1-\frac{x^2}{a'^2}+\frac{\bar{y}^2}{a'^2}\right]^2+4\frac{x^2}{a'^2}\frac{\bar{y}^2}{a'^2}}$$

are dimensionless values. It should be noted that

$$\sqrt{\frac{1}{2}\left[\lambda-\left(1-\frac{x^2}{a'^2}+\frac{\bar{y}^2}{a'^2}\right)\right]}$$

changes sign, the root being positive for $x < 0$ and negative for $x > 0$.

Denoting the integral J_n for the individual values of n with J_0, J_1, J_2, and J_3 while keeping $f_\nu(\xi/a')$ in mind, equation (65) gives

$$\left.\begin{aligned} P_1\left[f_1\left(\frac{\xi}{a'}\right)\right] &= J_0+2J_1; & P_2\left[f_1\left(\frac{\xi}{a'}\right)\right] &= J_1+2J_2 \\ P_1\left[f_2\left(\frac{\xi}{a'}\right)\right] &= J_0; & P_2\left[f_2\left(\frac{\xi}{a'}\right)\right] &= J_1 \\ P_1\left[f_3\left(\frac{\xi}{a'}\right)\right] &= J_0+J_1; & P_2\left[f_3\left(\frac{\xi}{a'}\right)\right] &= J_1+J_2 \end{aligned}\right\} \quad (71)$$

and

$$P_1\left[f_4\left(\frac{\xi}{a'}\right)\right] = J_1+J_2; \qquad P_2\left[f_4\left(\frac{\xi}{a'}\right)\right] = J_2+J_3$$

which, entered in (64), finally yields the dimensionless speed factors of the vortex distributions, as follows:

Along the x axis

$$\left.\begin{aligned} \frac{\partial W_2}{\partial y/a'} &= -\frac{\bar{y}}{a'}\left[\Omega_1+\left(1-\frac{x}{a'}\right)\Omega_2\right] \\ \frac{\partial W_3}{\partial y/a'} &= -\frac{\bar{y}}{a'}\left[1+2\frac{x}{a'}\Omega_1+\left(1-\frac{x^2}{a'^2}+\frac{\bar{y}^2}{a'^2}\right)\Omega_2\right] \\ \frac{\partial W_4}{\partial y/a'} &= -\frac{\bar{y}}{a'}\left[2\frac{x}{a'}+\left(\frac{x}{a'}\Omega_2-\Omega_1\right)\right. \\ &\quad \left.-\frac{x^2}{a'^2}\left(\frac{x}{a'}\Omega_2-3\Omega_1\right)+\frac{\bar{y}^2}{a'^2}\left(3\frac{x}{a'}\Omega_2-\Omega_1\right)\right] \end{aligned}\right\} \quad (72)$$

and along the y axis

$$\left.\begin{aligned} \frac{\partial W_2}{\partial x/a'} &= 1-\left(1-\frac{x}{a'}\right)\Omega_1+\frac{\bar{y}^2}{a'^2}\Omega_2 \\ \frac{\partial W_3}{\partial x/a'} &= \frac{x}{a'}-\left(1-\frac{x^2}{a'^2}\right)\Omega_1+\frac{\bar{y}^2}{a'^2}\left(2\frac{x}{a'}\Omega_2-\Omega_1\right) \\ \frac{\partial W_4}{\partial x/a'} &= -\left[\frac{1}{2}-\frac{x^2}{a'^2}+\frac{\bar{y}^2}{a'^2}+\frac{\bar{y}^2}{a'^2}\Omega_2+\frac{x}{a'}\Omega_1\right. \\ &\quad \left.-\frac{x^2}{a'^2}\left(3\frac{\bar{y}^2}{a'^2}\Omega_2+\frac{x}{a'}\Omega_1\right)+\frac{\bar{y}^2}{a'^2}\left(\frac{\bar{y}^2}{a'^2}\Omega_2+3\frac{x}{a'}\Omega_1\right)\right] \end{aligned}\right\} \quad (73)$$

The dimensionless speed values of the source distribution are obtained from those of the vortex distribution with (22) and (64). The value for the component along the x axis is

$$\frac{\partial Q_1}{\partial y/a'} = \frac{\partial W_2}{\partial x/a'} - 2\frac{\partial W_3}{\partial x/a'},$$

and that along the y axis

$$\frac{\partial Q_1}{\partial x/a'} = 2\frac{\partial W_3}{\partial y/a'} - \frac{\partial W_2}{\partial y/a'} \quad \ldots\ldots (74)$$

Now there is lacking only the speeds of the source-sink distribution of the crescent $\overline{f_5}\left(\frac{\xi}{a'}\right)$, (equation (42)), the flow function of which occupies a special position among the integrals. Its exact evaluation requires a numerical process, since $\overline{f_5}(\xi/a')$ is given as such (fig. 9)*. But, discounting the region in proximity of the branch points A_1' and A_2', the analytically given form $f_5(\xi/a')$ (equation (42a)), which is wrong only in the vicinity previously mentioned, can be used (shown by dashes in fig. 9). Then

$$\left.\begin{aligned} \frac{\partial Q_5}{\partial y/a'} &= -\frac{1}{\pi}\frac{1}{a'}\int_{-a'}^{+a'} \frac{x-\xi}{(x-\xi)^2+\bar{y}^2}\,\xi\,d\xi \\ \text{and} \\ \frac{\partial Q_5}{\partial x/a'} &= +\frac{1}{\pi}\frac{1}{a'}\int_{-a'}^{+a'} \frac{\bar{y}}{(x-\xi)^2+\bar{y}^2}\,\xi\,d\xi \end{aligned}\right\} \quad \ldots (75)$$

Solution of the two integrals

$$\int_{-a'}^{+a'} \frac{\xi\,d\xi}{(x-\xi)^2+\bar{y}^2} = \frac{1}{2}\ln\frac{(x-a')^2+\bar{y}^2}{(x+a')^2+\bar{y}^2} + \frac{x}{a'}\operatorname{arc\,tg}\frac{2a'\bar{y}}{x^2-a'^2+\bar{y}^2}$$

and

$$\frac{1}{a'}\int_{-a'}^{+a'} \frac{\xi^2\,d\xi}{(x-\xi)^2+\bar{y}^2} = 2 + \frac{x}{a'}\ln\frac{(x-a')^2+\bar{y}^2}{(x+a')^2+\bar{y}^2} + \frac{x^2-\bar{y}^2}{a'\bar{y}}\operatorname{arc\,tg}\frac{2a'\bar{y}}{x^2-a'^2+\bar{y}^2},$$

gives for the source distribution of the crescent the functions

$$\left.\begin{aligned} \frac{\partial Q_5}{\partial y/a'} &= \frac{1}{\pi}\left[2 + \frac{1}{2}\frac{x}{a'}\ln\frac{(x-a')^2+\bar{y}^2}{(x+a')^2+\bar{y}^2} - \frac{\bar{y}}{a'}\operatorname{arc\,tg}\frac{2a'\bar{y}}{x^2-a'^2+\bar{y}^2}\right] \\ \frac{\partial Q_5}{\partial x/a'} &= \frac{1}{\pi}\left[\frac{1}{2}\frac{\bar{y}}{a'}\ln\frac{(x-a')^2+\bar{y}^2}{(x+a')^2+\bar{y}^2} + \frac{x}{a'}\operatorname{arc\,tg}\frac{2a'\bar{y}}{x^2-a'^2+\bar{y}^2}\right] \end{aligned}\right\} \quad (76)$$

Herewith the dimensionless speed factors of all the singularity distributions are secured which, in first approximation, give the velocity field in the vicinity of a profile. The second part gives the velocity fields of every single singularity distribution in diagrams which enable easy reading of the values for each point. The individual values obtained by differentiation of equations (58) and (59) and allowance for (63), read as follows:

$$\begin{aligned} \frac{u\left(\frac{x}{a'};\frac{\bar{y}}{a'}\right)}{V_\infty} = \cos\alpha\Bigg[& 1 + \frac{d}{a}\frac{\partial Q_1\left(\frac{x}{a'};\frac{\bar{y}}{a'}\right)}{\partial y/a'} \\ & + \frac{1}{2}\delta\frac{\partial \overline{Q}_5\left(\frac{x}{a'},\frac{\bar{y}}{a'}\right)}{\partial y/a'} + 2\operatorname{tg}\beta\frac{\partial W_3\left(\frac{x}{a'};\frac{\bar{y}}{a'}\right)}{\partial y/a'} \\ & - \frac{\mu}{4}\left(\frac{\partial W_2\left(\frac{x}{a'};\frac{\bar{y}}{a'}\right)}{\partial y/a'} + 6\frac{\partial W_4\left(\frac{x}{a'};\frac{\bar{y}}{a'}\right)}{\partial y/a'}\right) + \frac{\partial g_x}{\partial y/a'}\Bigg] \\ & + \sin\alpha\Bigg[\left(1 + 2\frac{d}{a} + \varkappa\right)\frac{\partial W_2\left(\frac{x}{a'};\frac{\bar{y}}{a'}\right)}{\partial y/a'} \\ & - 2\frac{d}{a}\frac{\partial W_3\left(\frac{x}{a'};\frac{\bar{y}}{a'}\right)}{\partial y/a'} + \frac{\partial g_y}{\partial y/a'}\Bigg] \end{aligned} \quad (77)$$

speed in y axis direction

$$\begin{aligned} \frac{v\left(\frac{x}{a'},\frac{\bar{y}}{a'}\right)}{V_\infty} = \sin\alpha\Bigg[& 1 - \left(1 + 2\frac{d}{a} + \varkappa\right)\frac{\partial W_2\left(\frac{x}{a'};\frac{\bar{y}}{a'}\right)}{\partial \frac{x}{a'}} \\ & + 2\frac{d}{a}\frac{\partial W_3\left(\frac{x}{a'},\frac{\bar{y}}{a'}\right)}{\partial \frac{x}{a'}} - \frac{\partial g_y}{\partial \frac{x}{a'}}\Bigg] \\ & - \cos\alpha\Bigg[\frac{d}{a}\frac{\partial Q_1\left(\frac{x}{a'},\frac{\bar{y}}{a'}\right)}{\partial \frac{x}{a'}} + \frac{1}{2}\delta\frac{\partial Q_5\left(\frac{x}{a'},\frac{\bar{y}}{a'}\right)}{\partial \frac{x}{a'}} \\ & + 2\operatorname{tg}\beta\frac{\partial W_3\left(\frac{x}{a'};\frac{\bar{y}}{a'}\right)}{\partial \frac{x}{a'}} - \frac{\mu}{4}\left(\frac{\partial W_2\left(\frac{x}{a'};\frac{\bar{y}}{a'}\right)}{\partial \frac{x}{a'}} \right. \\ & \left. + 6\cdot\frac{\partial W_4\left(\frac{x}{a'},\frac{\bar{y}}{a'}\right)}{\partial \frac{x}{a'}}\right) + \frac{\partial g_x}{\partial \frac{x}{a'}}\Bigg] \end{aligned} \quad (78)$$

*The values $\overline{f_5}\left(\frac{\xi}{a'}\right)$ can, in good approximation, be considered linear in $\delta = \kappa\pi$ and are therefore plotted for $\delta = 1.0$.

Here also the terms with g_x and g_y are quadratic small (equations (82) and (83)) in the appendix.

Because of the cited omissions the formulas secured here are not applicable at the profile edge or its immediate vicinity, which, moreover, would exceed the purposes of the present work.

3. Appendix. The Quadratic Members of the Development

Since the singularity distributions were obtained by means of a development according to profile constants, the linear terms of the development will ordinarily be insufficient in closest proximity of the profile contour. This fact is of importance only when attempting to check the accuracy of a predetermined profile by the given distributions. But for predicting the velocity field in the neighborhood of a profile the linear terms should prove sufficient, whence in this case the quadratic terms give an error estimation.

Quoting all the quadratic terms secured would complicate the representation and entail hardly worth while paper work in the error estimation and the check on the profile contour. Hence the various nonessential terms are disregarded. These are the correction terms in equation (41), which secure new analytical expressions for the superposition density. They are themselves small as quadratic terms and produce minor, negligible changes in the distributions of the Joukowski profile due to the edge angle. The correction term in equation (42) alone remains, in order that this distribution portray the true conditions of the crescent of the Kármán-Trefftz profile. The additional integrals in (56a) and (56b) are discounted, as the new integral forms have only a slight effect on the results. All these terms can be disregarded for the very reason that the general profiles, for which ultimately the singularity distributions are used, mostly deviate from Kármán-Trefftz profiles from which the distributions have been obtained.

There remain then the quadratic terms of the singularity distributions of (16) to (19) and (34) to (36). Of these only the distributions multiplied by $V_x = V_\infty \cos \alpha$ are employed; the quadratic values multiplied by $V_y = V_\infty \sin \alpha$ are likewise ignored, as the angle of attack α is consistently presumed to be small.

Furthermore, while the wing chord is largely responsible for the flow in y-axis direction, that is, the vortex distribution of the flat plate (equation (24)) the thickness and camber of the profile are of secondary importance. In consequence, only the singularity distributions are written that appear for the flow in x axis direction, as they alone contribute a perceptible share to the results. They are the source distributions

$$\left.\begin{aligned} q_1^{(2)}\left(\frac{\xi}{a'}\right) &= -2\,V_x\,\frac{d}{a}\left(2\,\frac{d}{a}+\kappa\right) f_1\left(\frac{\xi}{a'}\right) \\ q_4^{(2)}\left(\frac{\xi}{a'}\right) &= +12\,V_x\,\frac{d^2}{a^2}\,f_4\left(\frac{\xi}{a'}\right) \\ \bar{q}_5^{(2)}\left(\frac{\xi}{a'}\right) &= -\frac{3}{2}\,V_x\,\delta\kappa\,\bar{f}_5\left(\frac{\xi}{a'}\right) \end{aligned}\right\} \qquad (79)$$

of which the source distribution $f_4\left(\frac{\xi}{a'}\right)$ did not appear previously but will gain significance for the design of new profile forms because of its property of shifting the area of maximum thickness of a profile more toward profile center (II, 5). Distributions $q_1^{(2)}\left(\frac{\xi}{a'}\right)$ and $\bar{q}_5^{(2)}\left(\frac{\xi}{a'}\right)$ afford a correction to the contour of the Joukowski profile and the crescent, respectively. Because of the thickness effect on the camber the vortex distributions

$$\left.\begin{aligned} \gamma_2^{(2)}\left(\frac{\xi}{a'}\right) &= -2\,V_x\,\frac{d}{a}\,\tan\beta\,f_2\left(\frac{\xi}{a'}\right) \\ \gamma_3^{(2)}\left(\frac{\xi}{a'}\right) &= +4\,V_x\left(2\,\frac{d}{a}+\kappa\right)\tan\beta\,f_3\left(\frac{\xi}{a'}\right) \\ \gamma_4^{(2)}\left(\frac{\xi}{a'}\right) &= -12\,V_x\,\frac{d}{a}\,\tan\beta\,f_4\left(\frac{\xi}{a'}\right) \end{aligned}\right\} \qquad (80)$$

are additive to the corrections. Without these quadratic small terms (80) the profile on the side facing the curvature radius of the mean line would be thicker than on the

other (fig. 21): that is, the profile would apparently have a smaller camber.

In this manner the correction term for the streamline of the profile by V_x flow is obtained:

$$g_x = \frac{d}{a}\left(2\frac{d}{a}+\kappa\right)Q_1\left(\frac{x}{a'};\frac{\bar{y}}{a'}\right) - 6\frac{d^2}{a^2}Q_4\left(\frac{x}{a'};\frac{\bar{y}}{a'}\right)$$

$$+\frac{3}{4}\kappa\delta\bar{Q}_5\left(\frac{x}{a'};\frac{\bar{y}}{a'}\right) - \frac{d}{a}\tan\beta\left[W_2\left(\frac{x}{a'};\frac{\bar{y}}{a'}\right) - W_2(1;0)\right]$$

$$+2\left(2\frac{d}{a}+\kappa\right)\tan\beta\left[W_3\left(\frac{x}{a'};\frac{\bar{y}}{a'}\right) - W_3(1;0)\right]$$

$$-6\frac{d}{a}\tan\beta\left[W_4\left(\frac{x}{a'};\frac{\bar{y}}{a'}\right) - W_4(1;0)\right] + \qquad (81)$$

and inserted in equation (58), while g_y (equation (59)) is being disregarded.

Differentiation of this equation affords the quadratic small portions to the speeds in equations (77) and (78):

$$\frac{\partial g_x}{\partial y/a'} = \frac{d}{a}\left(2\frac{d}{a}+\kappa\right)\frac{\partial Q_1\left(\frac{x}{a'};\frac{\bar{y}}{a'}\right)}{\partial y/a'} - 6\frac{d^2}{a^2}\frac{\partial Q_4\left(\frac{x}{a'};\frac{\bar{y}}{a'}\right)}{\partial y/a'}$$

$$+\frac{3}{4}\kappa\delta\frac{\partial\bar{Q}_5\left(\frac{x}{a'};\frac{\bar{y}}{a'}\right)}{\partial y/a'} - \frac{d}{a}\tan\beta\frac{\partial W_2\left(\frac{x}{a'};\frac{\bar{y}}{a'}\right)}{\partial y/a'}$$

$$+2\left(2\frac{d}{a}+\kappa\right)\tan\beta\frac{\partial W_3\left(\frac{x}{a'};\frac{\bar{y}}{a'}\right)}{\partial y/a'} - 6\frac{d}{a}\tan\beta\frac{\partial W_4\left(\frac{x}{a'};\frac{\bar{y}}{a'}\right)}{\partial y/a'} \qquad (82)$$

and

$$\frac{\partial g_x}{\partial x/a'} = \frac{d}{a}\left(2\frac{d}{a} + \kappa\right)\frac{\partial Q_1\left(\frac{x}{a'};\frac{\bar{y}}{a'}\right)}{\partial x/a'} - 6\frac{d^2}{a^2}\frac{\partial Q_4\left(\frac{x}{a'};\frac{\bar{y}}{a'}\right)}{\partial x/a'}$$

$$+ \frac{3}{4}\kappa\delta\frac{\partial \bar{Q}_5\left(\frac{x}{a'};\frac{\bar{y}}{a'}\right)}{\partial x/a'} - \frac{d}{a}\tan\beta\frac{\partial W_2\left(\frac{x}{a'};\frac{\bar{y}}{a'}\right)}{\partial x/a'}$$

$$+ 2\left(2\frac{d}{a} + \kappa\right)\tan\beta\frac{\partial W_3\left(\frac{x}{a'};\frac{\bar{y}}{a'}\right)}{\partial x/a'} - 6\frac{d}{a}\tan\beta\frac{\partial W_4\left(\frac{x}{a'};\frac{\bar{y}}{a'}\right)}{\partial x/a'} \quad (83)$$

the individual terms of which are known from the linear distributions (equations (72) to (74)). Newly added are the speeds of the source distribution $f_4\left(\frac{\xi}{a'}\right)$ which, however, can be derived from those of the known vortex distribution for the S-shaped mean line, according to equation (64). Because

$$\frac{\partial Q_4\left(\frac{x}{a'};\frac{\bar{y}}{a'}\right)}{\partial y/a'} = -\frac{\partial W_4\left(\frac{x}{a'};\frac{\bar{y}}{a'}\right)}{\partial x/a'} \quad (84)$$

and

$$\frac{\partial Q_4\left(\frac{x}{a'};\frac{\bar{y}}{a'}\right)}{\partial x/a'} = \frac{\partial W_4\left(\frac{x}{a'};\frac{\bar{y}}{a'}\right)}{\partial y/a'} \quad (85)$$

The terms $\frac{\partial g_y}{\partial y/a'}$ and $\frac{\partial g_y}{\partial x/a'}$ are disregarded conformally to the foregoing arguments.

II. APPLICATION

1. Generalities

The solution of the singularity distributions for a generalized Kármán-Trefftz profile (reference 3) is described in part I of this report. The outstanding fact

is that the vortex and source distributions necessary for the substitution of a profile can be combined from only five different distributions $f_\nu\left(\frac{\xi}{a'}\right)$ indicating the abscissa of one singularity. To make the calculation as much as possible independent of the angle of attack α the parallel flow $V_\infty e^{-i\alpha}$ is divided into its component $V_x = V_\infty \cos\alpha$ along the x axis and its component $V_y = V_\infty \sin\alpha$ along the y axis. The first result is the vortex distributions as previously given by Birnbaum (fig. 10): the vortex distributions $2\,V_y\,f_2\left(\frac{\xi}{a'}\right)$ of the flat plate, the vortex distributions $4\,V_x \tan\beta\, f_3\left(\frac{\xi}{a'}\right)$ of the curved plate, the vortex distribution $-3\,V_x\,\mu\,f_4\left(\frac{\xi}{a'}\right)$ of S-profile.* These distributions are supplemented by two new source distributions (fig. 11) which appear only for the flow V_x. The one source distribution $-2\,V_x\,\frac{d}{a}\,f_1\left(\frac{\xi}{a'}\right)$ leads to a closed streamline similar to the symmetrical Joukowski profile, where $\frac{d}{a}$ is the parameter for the profile thickness. For the Kármán-Trefftz profiles with finite angle δ at the trailing edge the source distribution $-V_x\,\delta\,\overline{f_5}\left(\frac{\xi}{a'}\right)$ is additive; which, considered by itself, is the source distribution of a symmetrical crescent with edge angle δ (fig. 11).** Besides these singularity distributions generalized Kármán-Trefftz profiles have still other distributions composed of these five basic functions, which must be combined with the afore-mentioned superpositions and with the parallel flow according to a certain law if the Kármán-Trefftz profile is to be streamline in parallel flow.

---

*Constants $\tan\beta$, μ, $\frac{d}{a}$, and δ are discussed farther on.

**$\epsilon\left(\frac{\xi}{a'}\right)$ is explained in I, 1 b; for the rest, the graph affords a satisfactory representation of the aspect of $\overline{f_5}\left(\frac{\xi}{a'}\right)$.

Then, in order to establish the effect of any one of the singularity distributions on the flow formation or the speeds at a point of the plane of the section, the effect of all its singularity elements at this point must be summated, that is, integrated along the line on which they are located. The mean line of the profile is chosen as the depository of all singularities. During the development of the integral it was found that the ordinate $\frac{\eta}{a'}$ of the mean line (fig. 8) could be disregarded, and the singularities themselves assumed on the x axis, with a much simpler evaluation as a result. With $\frac{y_s}{a'}$ as the ordinate of the mean line, the point of the profile plane is given by

$$\frac{\bar{y}}{a'} = \frac{y}{a'} - \frac{y_s}{a'} \tag{86}$$

with $\frac{y}{a'}$ denoting the distance of this point from the x axis (fig. 12). For starting points at greater distance from the profile, put $\frac{\bar{y}}{a'} \approx \frac{y}{a'}$, that is, let the mean line and the coordinate axis coincide; but the two values must be carefully differentiated in profile proximity.

When in the following a method for computing the plane potential flow about general thick wing profiles is evolved, it is practical to utilize fully the data secured for the generalized Kármán–Trefftz profile, since the flow condition for each of these profiles is known. As the calculation is to deal with the flow about a general profile in the neighborhood of the profile but not on its surface, the method can be restricted to an approximation, that is, the given general profile is closely substituted by a generalized Kármán–Trefftz profile, which merely stipulates knowing the profile constants for this similar Kármán–Trefftz profile, which then is a good approximation for nearly all practical profile forms. The substituting singularities of this profile are herewith known, and it will not be necessary as a rule to check on the given profile the extent to which it is represented by the singularities.

The reason for checking the profile contour (II, 3)

is simply in order to show how closely the contour of general profiles agrees with the closed streamline of the approximately resolved flow.

But the singularity distributions afford, in addition, still other new profile forms with certain, predetermined profile characteristics. They may even vary substantially from those of the Kármán–Trefftz profiles if provision is made that the singularity distributions characteristic for certain profile forms are combined in a manner other than that prescribed for the Kármán–Trefftz profile. The profile contour is computed from the singularity distributions analogous to the method employed by Fuhrmann (reference 6) to airship hulls. By the determination of the velocity field of these profiles the pressure distribution can be indicated also in good approximation.*

2. Determination of the Profile Constants

The generalized Kármán–Trefftz profile is completely defined by four profile constants. But before the calculation can be made the mean line and the axis of the Kármán–Trefftz profile must be plotted first in the given general profile, which agrees with the mean line of the general profile only for symmetrical profiles. The mean line of the section is closely approximated by the line connecting the centers of all the circles which touch the profile contour twice from the inside (fig. 13), the curvature circle (radius ρ) on the nose included. The axis of the Kármán–Trefftz profile which at the same time is the x axis of the plane of the section is given by two points A_1' and A_2' (fig. 13). Point A_1', located at the section tip, forms the vertex of the pointed trailing edge; for sections rounded off aft** of the rear contact point of the tangent to the section lower surface, of the chord, with the section is chosen. Point A_2' is located at half curvature radius $\left(\frac{\rho}{2}\right)$ from the nose on the mean line.*** Distance $A_1'A_2'$ is put equal to $2a'$.

---

*Although it affords the closed streamline for the flow in x direction exact, the vortex distributions for the flow in y direction can only be approximately determined.

**Strictly speaking, it should be constructed just like point A_1' at the nose.

***Herewith the position of point A_2' is accurately enough defined; although the plotting of the curvature circle is afflicted with a certain error.

The geometric angle of attack α_g does not, in general, agree with the angle of attack α which must be measured from the x axis. With α_s denoting the angle between x axis and profile chord ($\alpha_g = 0$) (fig. 13):

$$\alpha = \alpha_g + \alpha_s \tag{87}$$

The ordinate axis, axis y, of the profile is the median vertical on the length $\overline{A_1' A_2'}$.

Quantities $\tan \beta$ and μ giving the camber and the reversed curvature are obtained from the ordinates of the mean line and not from the tangents (as Birnbaum did) which cannot be accurately plotted. For generalized Kármán-Trefftz profiles the mean line is, in good approximation, a curve of the third degree (equation (53)) through points $A_1'A_2'$, with which the general profile must coincide in two additional points. Choosing the points at $\frac{x}{a'} = -0.5$ with the ordinate $\frac{y_2}{a'}$ and at $\frac{x}{a'} = 0.5$ with the ordinate $\frac{y_1}{a'}$ (fig. 14) affords*

1. The index for the camber

$$\tan \beta = \frac{2}{3}\left(\frac{y_2}{a'} + \frac{y_1}{a'}\right) \tag{88}$$

2. The index for the reversed curvature

$$\mu = \frac{8}{3}\left(\frac{y_2}{a'} - \frac{y_1}{a'}\right) \tag{89}$$

This secures the quantities which define the intensity of the vortex distributions for the curved S-shaped mean line.

The two remaining profile constants of the generalized Kármán-Trefftz profile must be computed from the thickness curve of the profile; whereas a Joukowski profile requires only a section constant d/a for the thickness, the finite trailing edge angle δ on the Kármán-Trefftz profiles affects the thickness at every point, particularly, a profile of finite thickness, the crescent

*See also: equation (54) and the context.

is left over for $\frac{d}{a} = 0$. Therefore, the thickness of a Karman–Trefftz profile is defined by two criterions, δ and $\frac{d}{a}$, the magntiude of which is not ascertainable from the plotted profile without specified assumptions. If δ were given the value of $\frac{d}{a}$ (denoted with $\frac{O_1O_2}{a}$ by Betz–Keune) could be deduced from the thickness at profile center by the Betz–Keune method (reference 3, equation (2)); but it is found that δ cannot be accurately enough defined from the angle at the trailing edge, because the effect of the constant $\frac{d}{a}$ on the profile thickness starts too close to the trailing edge, as is readily seen from the Kármán–Trefftz profiles.* Therefore, δ and $\frac{d}{a}$ had to be secured in a different way. Since the thickness remains approximately independent of the camber and the S curvature (see equation (2) of reference (3)) and since the symmetrical Kármán–Trefftz profile acts, in good approximation, as if the ordinates of the crescent with the edge angle δ and the ordinates of the Joukowski profile with the criterion $\frac{d}{a}$ were additive,** the profile constants can be expressed by approximate formulas. If profile criterions are employed again at $\frac{x}{a'} = \pm 0.5$, it then is expedient to denote $\frac{D_1}{a'}$, as thickness at $\frac{x}{a'} = 0.5$ and $\frac{D_2}{a'}$ as thickness at $\frac{x}{a'} = -0.5$ (fig. 14).

Then δ follows at

$$\frac{d}{a} \approx \frac{1}{3}\left(\frac{D_2}{a'} - \frac{D_1}{a'}\right)\left[\sqrt{3} + \left(\frac{D_2}{a'} - \frac{D_1}{a'}\right)\right] \tag{90}$$

and δ, in radians, at

---

*Angle δ at the trailing edge is read off as much as 80 percent too great.

**For the symmetric Joukowski profile and the crescent the ordinates in each point are easily secured, but that for the Kármán–Trefftz profile is very complicated.

$$\delta \approx \frac{4}{3}\left(3\frac{D_1}{a'} - \frac{D_2}{a'}\right) \tag{91}$$

Although these formulas are not exact, equation (90) proved very satisfactory in a check on a large number of Kármán-Trefftz profiles, and equation (91) agrees with the correct values up to $\approx 1^0$. Since equation (90) is independent of δ, an error in δ is of little consequence on the subsequent results. With these constants the aerodynamic characteristics of generalized Kármán-Trefftz profiles themselves are secured. These relations also hold, approximately, for general profiles with the same constants. The theoretical lift is

$$c_a \approx \frac{2}{t/a'} 2\pi\left(1 + \frac{1}{2}\frac{\delta}{\pi} + \frac{d}{a}\right)\sin\left(\alpha + \beta - \frac{1}{4}\mu\right) \tag{92}$$

where $\frac{4\pi a'}{t}\left(1 + \frac{1}{2}\frac{\delta}{\pi} + \frac{d}{a}\right)$ is the theoretical lift gradient that is always greater than the true value, because the friction is not taken into account, and $\alpha_0 = -\left(\beta - \frac{1}{4}\mu\right)$ is the zero lift angle of this profile, measured from the x axis. The moment coefficient, referred to the centroid F of the profile, is (see reference 3, p. 341)

$$c_{m_F} \approx \frac{\pi\left(1 - \frac{1}{3}\frac{\delta}{\pi}\right)}{t^2/a'^2}\sin 2\left(\beta - \frac{3}{8}\mu\right) \tag{93}$$

The profile has a fixed center of pressure, when $\mu_1 \approx \frac{8}{3}\beta$.*

3. Substitution of a Given Profile by Singularities

In a check on the extent to which the generalized Kármán-Trefftz profile obtained by the computed constants agrees with the given general profile, the study can be limited to the profile in parallel flow along the x axis. The parallel flow along the y axis is essentially affected by the vortex distribution of the flat plate into which the profile chord enters. Against this effect the dis-

*See reference 3, equation (48), where, however, the squared terms are taken into account.

tributions due to profile thickness or to the mean line are inferior, especially since V_y always remains smaller than $V_x (V_y \ll V_x)$; hence the approximation of the profile by one of the Kármán–Trefftz type should always remain accurately enough in this direction of flow.

For the flow along the x axis the streamline equation (58) – if the closed streamline is given the value $\frac{\Psi_x}{a' V_x} = 0$ * – affords

$$-\frac{y}{a'} = +\frac{d}{a} Q_1\left(\frac{x}{a'};\frac{\bar{y}}{a'}\right) + \frac{1}{2}\,\partial\, \bar{Q}_5\left(\frac{x}{a'};\frac{\bar{y}}{a'}\right)$$

$$+2\tan\beta\left[W_3\left(\frac{x}{a'};\frac{\bar{y}}{a'}\right) - W_3(1;0)\right] - \frac{\mu}{4}\left\{\left[W_2\left(\frac{x}{a'};\frac{\bar{y}}{a'}\right) - W_2(1;0)\right]\right.$$

$$\left. +6\left[W_4\left(\frac{x}{a'};\frac{\bar{y}}{a'}\right) - W_4(1;0)\right]\right\} + g_x \qquad (94)$$

Here $Q_\nu\left(\frac{x}{a'};\frac{\bar{y}}{a'}\right)$ and $W_\nu\left(\frac{x}{a'};\frac{\bar{y}}{a'}\right)$ are, according to equations (60) and (61), the abbreviations of the integrals of the flow function of the respective source-sink and vortex distributions $f_\nu\left(\frac{\xi}{a'}\right)$. The subscript ν of $f_\nu\left(\frac{\xi}{a'}\right)$ is always in agreement with that of Q_ν and W_ν. These integrals have been evaluated for all necessary values $\frac{x}{a'}$ and $\frac{\bar{y}}{a'}$ and the results plotted in figures 15 to 19 against $\frac{\bar{y}}{a'}$ for fixed abscissas $\frac{x}{a'}$ and tabulated in tables 1 to 5. Allowance for the squared term g_x

---

*Provided this streamline in the rear stagnation point of the profile $A_1'\left(\frac{x}{a'} = +1.0;\ \frac{y}{a'} = 0\right)$ reaches the value $\frac{\Psi_x}{a' V_x} = 0$. This is achieved with the aid of the constants $W_2(1;0)$, $W_3(1;0)$, and $W_4(1;0)$.

$$g_x = \frac{d}{a}\left(2\frac{d}{a} + \kappa\right)Q_1\left(\frac{x}{a'};\frac{\bar{y}}{a'}\right) - 6\frac{d^2}{a^2}Q_4\left(\frac{x}{a'};\frac{\bar{y}}{a'}\right)$$

$$+ \frac{3}{4}\kappa\delta\bar{Q}_5\left(\frac{x}{a'};\frac{\bar{y}}{a'}\right) - \frac{d}{a}\tan\beta\left[W_2\left(\frac{x}{a'};\frac{\bar{y}}{a'}\right) - W_2(1;0)\right]$$

$$+ 2\left(2\frac{d}{a} + \kappa\right)\tan\beta\left[W_3\left(\frac{x}{a'};\frac{\bar{y}}{a'}\right) - W_3(1;0)\right]$$

$$- 6\frac{d}{a}\tan\beta\left[W_4\left(\frac{x}{a'};\frac{\bar{y}}{a'}\right) - W_4(1;0)\right] \qquad (94a)$$

adds the integral $Q_4\left(\frac{x}{a'};\frac{\bar{y}}{a'}\right)$ of the source-sink distribution $f_4(\xi/a')$ the values of which are shown in figure 20 and table 6. The squared term is usually needed in a check of the profile contour.

The streamline simulated by the singularities is defined by approximation on the assumption that the given profile actually has become the streamline through the computed profile constants $\tan\beta$, μ, $\frac{d}{a}$, and δ (equations (88) to (91)). In this instance the right- and left-hand sides of equation (94) would have to agree. Then the successive entry of the coordinates of individual points of the profile contour in the right-hand side of (94) with due allowance for (86) - the values of the integrals $Q_\nu\left(\frac{x}{a'};\frac{\bar{y}}{a'}\right)$ and $W_\nu\left(\frac{x}{a'};\frac{\bar{y}}{a'}\right)$ being read from figures 15 to 20, and the calculation proceeding in this manner with (94) - ultimately affords a value, which shall be expressed with $-\left(\frac{y}{a'}\right)_\Psi$. It affords already a very good approximation for the ordinate $\left(\frac{\bar{y}}{a'}\right)_\Psi$ of the closed streamline $\Psi_x = 0$.

Since all singularity distributions were directly derived for the contour of a generalized Kármán-Trefftz profile, the form of the given profiles is approximately

always complied with by the singularities. Hence, no pecularities are anticipated at any profile points, and it is sufficient to compute the ordinates of the streamline in a few points.

The method is first checked on three Kármán-Trefftz profiles (fig. 21) constructed according to the Betz-Keune method (reference 3) with the profile constants given in figure 21.* The constants are computed according to equations (88) to (91) and the values posted in equation (94). The result is

First profile:

$$\left(\frac{D_{max}}{t} = 0.138\right) \left| \frac{D_2}{a'} = 0.272; \quad \frac{D_1}{a'} = 0.130; \quad \frac{y_2}{a'} = \frac{y_1}{a'} = 0.0 \right.$$

$$\frac{d}{a} = 0.089; \quad \delta = 9^\circ \qquad \tan \beta = 0; \quad \mu = 0$$

Second profile:

$$\left(\frac{D_{max}}{t} = 0.120\right) \left| \frac{D_2}{a'} = 0.234; \quad \frac{D_1}{a'} = 0.112; \quad \frac{y_2}{a'} = \frac{y_1}{a'} = 0.038 \right.$$

$$\frac{d}{a} = 0.075; \quad \delta = 8^\circ \qquad \tan \beta = 0.051; \quad \mu = 0$$

Third profile:

$$\left(\frac{D_{max}}{t} = 0.195\right) \left| \frac{D_2}{a'} = 0.398; \quad \frac{D_1}{a'} = 0.130; \quad \frac{y_2}{a'} = \frac{y_1}{a'} = 0.066 \right.$$

$$\frac{d}{a} = 0.15; \quad \delta = 8^\circ \qquad \tan \beta = 0.088; \quad \mu = 0$$

Comparison of these values with those in figure 21 shows a slight error in edge angle, which, however, is scarcely noticeable in the calculation since the effect of thickness d/a is much more decisive for the profile contour. Figure 21 indicates that the second approximation (squared term g_x accounted for) is a very good check, even for great thickness, of the extent to which a given profile agrees with the Kármán-Trefftz profile.

As an example for general profiles, three NACA profiles are selected (reference 7) and first the profile constants are computed (see fig. 22):

---

* $\frac{d}{a} = \frac{\overline{O_1O_2}}{a}$ and $\tan \beta = \frac{\overline{OO_1}}{a}$ in reference 3.

NACA 2412:

$$\frac{D_2}{a'} = 0.241; \quad \frac{D_1}{a'} = 0.125; \quad \frac{y_2}{a'} = 0.0323; \quad \frac{y_1}{a'} = 0.0246$$

$$\frac{d}{a} = 0.072; \quad \delta = 10^\circ \qquad \tan\beta = 0.038; \quad \mu = 0.021$$

NACA 2712:

$$\frac{D_2}{a'} = 0.240; \quad \frac{D_1}{a'} = 0.129; \quad \frac{y_2}{a'} = 0.0242; \quad \frac{y_1}{a'} = 0.384$$

$$\frac{d}{a} = 0.068; \quad \delta = 11^\circ \qquad \tan\beta = 0.042; \quad \mu = -0.038$$

NACA 4418:

$$\frac{D_2}{a'} = 0.386; \quad \frac{D_1}{a'} = 0.190; \quad \frac{y_2}{a'} = 0.0667; \quad \frac{y_1}{a'} = 0.0525$$

$$\frac{d}{a} = 0.109; \quad \delta = 16^\circ \qquad \tan\beta = 0.08; \quad \mu = 0.038.$$

To explain the calculation method, the calculation of $\left(\frac{y}{a'}\right)_\Psi$ is carried out for a point of the NACA 2412 airfoil section. The profile point selected is $\frac{x}{a'} = -0.5$; $\frac{\bar{y}}{a'} = 0.153$. Then (86)

$\frac{\bar{y}}{a'} = 0.153 - 0.032 = 0.121$ and there is obtained

$$Q_1(-0.5;\ 0.121) = -1.11 \qquad W_2(-0.5;\ 0.121) = -0.308$$

$$\bar{Q}_5(-0.5;\ 0.121) = -0.298 \qquad W_3(-0.5;\ 0.121) = -0.033$$

$$[Q_4(-0.5;\ 0.121) = -0.195] \qquad W_4(-0.5;\ 0.121) = 0.167$$

$$W_2(1.0;0) = 1.0; \quad W_3(1.0;0) = 0.25; \quad W_4(1.0;0) = -0.166$$

wherewith equation (94) gives: $-\left(\frac{y}{a'}\right)_\Psi = -0.131 + g_x$.

The accord with the ordinate of the profile point is still unsatisfactory. With the quadratic term (equation (94a)) $g_x = -0.018$ becomes $\left(\frac{y}{a'}\right)_\Psi = 0.149$ and affords a sat-

isfactory agreement between profile point and streamline of the related generalized Kármán-Trefftz profile. The same procedure is followed at the other points of the section contour. The results, plotted in figures 21 and 22 manifest satisfactory agreement at all points.

4. The Velocity Field of a Given Profile

The singularity distributions on the mean line of a profile induce at each point $P\left(\frac{x}{a'}\ \frac{y}{a'}\right)$, (fig. 23), a speed $\underline{w} = w\, e^{i\vartheta}$, the slope of which toward the positive x axis ϑ and the absolute amount $|\underline{w}| = w$. The amount and the angle follow from the components parallel to the coordinate axes as follows:

$$\frac{w}{V_\infty} = \sqrt{\left(\frac{u}{V_\infty}\right)^2 + \left(\frac{v}{V_\infty}\right)^2} \approx \frac{u}{V_\infty}\left(1 + \frac{1}{2}\vartheta^2\right) \tag{95}$$

and

$$\vartheta = (\tan^{-1})\ \frac{v}{u} \approx \frac{v}{u} \tag{96}$$

The speed components $\frac{u}{V_\infty}$ and $\frac{v}{V_\infty}$ are obtained by differentiation of the equation of the flow function $\psi/a'\,V_\infty$ with respect to $\frac{y}{a'}$ and $\frac{x}{a'}$, being composed of the differential quotients of the flow function $\psi_x/a'\,V_\infty$ obtained for the flow along the x axis and the flow function $\psi_y/a'\,V_\infty$ along the y axis; it is:

$$\left.\begin{aligned} \frac{u}{V_\infty} &= \cos\alpha\left[\frac{\partial\ \frac{\psi_x}{a'\,V_\infty}}{\partial\ y/a'} + \frac{\partial\ \frac{\psi_y}{a'\,V_\infty}}{p\ y/a'}\tan\alpha\right] \\ \frac{v}{V_\infty} &= -\cos\alpha\left[\frac{\partial\ \frac{\psi_x}{a'\,V_\infty}}{\partial\ x/a'} + \frac{\partial\ \frac{\psi_y}{a'\,V_\infty}}{\partial\ x/a'}\tan\alpha\right] \end{aligned}\right\} \tag{97}$$

The speeds $\frac{u}{V_\infty}$ and $\frac{v}{V_\infty}$, being thus known from from equa-

tions (58) and (59), can be defined by the method given in the tabulation. Each source and vortex distribution composed of $f_\nu\left(\frac{\xi}{a'}\right)$ and $\tan\beta$, μ, $\frac{d}{a}$ and δ, contributes its share to the speeds (made dimensionless with V_∞) at a point $P\left(\frac{x}{a'};\frac{\bar{y}}{a'}\right)$, for the source distributions

$$\frac{\partial\, Q_\nu\left(\frac{x}{a'};\frac{\bar{y}}{a'}\right)}{\partial\, y/a'} \quad \text{along the x axis and}$$

$$\frac{\partial\, Q_\nu\left(\frac{x}{a'};\frac{\bar{y}}{a'}\right)}{\partial\, x/a'} \quad \text{along the y axis}$$

Correspondingly the vortex distributions are

$$\frac{\partial\, W_\nu\left(\frac{x}{a'};\frac{\bar{y}}{a'}\right)}{\partial\, y/a'} \quad \text{and} \quad \frac{\partial\, W_\nu\left(\frac{x}{a'};\frac{\bar{y}}{a'}\right)}{\partial\, x/a'}$$

Thus it affords, according to the tabulation, for example:

$$\frac{\partial\, \frac{\Psi_x}{a' V_\infty}}{\partial\, y/a'} = 1 + \frac{d}{a}\,\frac{\partial\, Q_1\left(\frac{x}{a'};\frac{\bar{y}}{a'}\right)}{\partial\, y/a'} + \ldots.$$

The velocity field for each of the five singularity distribution is shown in figures 24 to 28, the lines of constant speed in x and y direction being connected in a system, from which the speed portions of a selected singularity distribution for each point can be read off.* The calculation of the correction terms is usually unnecessary, since they merely afford an error estimation and are given in (82) and (83) simply for the sake of completeness. One exception is the quadratic term $\frac{\partial\, g_x}{\partial\, x/a'}$, which essentially affects the direction of the

*Because of the necessary additive term (equation (42)), the speeds in the vortex distribution $\bar{f}_5\left(\frac{\xi}{a'}\right)$ (fig. 25), were obtained by numerical integration.

speed. This is due to the fact that the speed $\frac{\partial \Psi_x/a' V_\infty}{\partial x/a'}$ to be multiplied by $\cos\alpha$ begins with terms already small of the first order. Here $\frac{\partial g_x}{\partial x/a'}$ is of the same order of magnitude as the linear terms of $\tan\alpha \frac{\partial \Psi_y/a' V_\infty}{\partial x/a'}$.

As an example, take the velocity field of the Göttingen 624 airfoil section (reference 8) (see fig. 29). Computing the profile constants by equations (88) to (91) affords, with

$$\frac{D_2}{a'} = 0.319; \quad \frac{D_1}{a'} = 0.160$$

$$\frac{y_2}{a'} = 0.102; \quad \frac{y_1}{a'} = 0.062$$

the values

$$\frac{d}{a} = 0.10; \quad \delta = 12^\circ; \quad \kappa = \frac{\delta}{\pi} = 0.067; \quad \tan\beta = 0.109; \quad \mu = 0.107$$

hence for the zero lift angle: $-\alpha_0 = \beta - \frac{1}{4}\mu$; $\alpha_0 = -4.65^\circ$. Since the profile chord slopes at angle $\alpha_s = 2.2^\circ$ toward the x axis, it is found (equation (87)) that the zero lift angle $\alpha_{0g} = -4.7^\circ - 2.2^\circ - 6.9^\circ$ is in complete agreement with the experimental value.

The speeds at a point of the plane of the section with coordinates $\frac{x}{a'} = -0.5$ and $\frac{\bar{y}}{a'} = -0.3$ are to be computed. Figures 24 to 28 give

$$\frac{\partial Q_1}{\partial y/a'} = 1.1 \quad \frac{\partial \bar{Q}_5}{\partial y/a'} = 0.23 \quad \frac{\partial W_2}{\partial y/a'} = -1.52$$

$$\frac{\partial W_3}{\partial y/a'} = 0.63 \quad \frac{\partial W_4}{\partial y/a'} = 0.21$$

$$\frac{\partial Q_1}{\partial x/a'} = 0.25 \quad \frac{\partial \bar{Q}_5}{\partial x/a'} = 0.31 \quad \frac{\partial W_2}{\partial x/a'} = 0.42$$

$$\frac{\partial W_3}{\partial x/a'} = 0.34 \quad \frac{\partial W_4}{\partial x/a'} = -0.15$$

for which the tabulation accordingly shows the following:

$$\frac{u}{V_\infty} = \cos\alpha\,[1.006 + -1.806\tan\alpha]$$

$$\frac{v}{V_\infty} = -\cos\alpha\,[-0.005 - 0.397\tan\alpha] - \frac{\partial g_x}{\partial x/a'}\cos\alpha$$

and

$$\frac{\partial g_x}{\partial x/a'} = -0.018$$

The only quadratic term to be considered in the calculation is $\frac{\partial g_x}{\partial x/a'}$. For the mean line alone, which up to now indicated the substitution of the profile according to Birnbaum, the same calculation method yields

$$\frac{u}{V_\infty} = \cos\alpha\,[0.871 + -1.52\tan\alpha]$$

$$\frac{v}{V_\infty} = -\cos\alpha\,[-0.062 - 0.58\tan\alpha] - \frac{\partial g_x}{\partial x/a'}\cos\alpha$$

and

$$\frac{\partial g_x}{\partial x/a'} = 0$$

With $\alpha = 3.4^\circ$ for the angle of attack which, according to (92), gives the lift $c_a = 1.0$, and the profile thickness taken into consideration, it is found that

$$\frac{u}{V_\infty} = 0.897;\quad \frac{v}{V_\infty} = 0.029 + 0.018 = 0.047$$

and for the mean line alone, according to Birnbaum's more convenient method in this instance

$$\frac{u}{V_\infty} = 0.779;\quad \frac{v}{V_\infty} = 0.097$$

This calculation is continued for other ordinates $\frac{\bar{y}}{a'}$ at point $\frac{x}{a'} = -0.5$, with added choice of angle of attack

$\alpha = -4.65°(c_a = 0)$ and $\alpha = -0.7°(c_a = 0.5)$. The results are shown plotted against $\bar{y}/a'$ in figure 30; whereas figures 31 and 32 shows other sections for $\frac{x}{a'} =$ constant. In all these graphs Birnbaum's approximation is indicated with dashes. The solid curves give the values with profile thickness allowed for, including the quadratic term $\frac{\partial g_x}{\partial x/a'}$. In the dash-dot curves this term has been discounted. In figures 30 and 31 the velocities were not computed up to the profile contour because the approximation is no longer applicable there. It is thus readily seen that the effect of profile thickness is in many cases quite pronounced. The discrepancies are even more pronounced near the nose where the location of the forward stagnation point by the Birnbaum approximation becomes very inaccurate, and infinite velocities occur at the mean line on flowing past the leading edge.

5. Appendix: Structure of New Profile Forms

In the ensuing development of new profile forms the computed source distributions of the Karman-Trefftz profile are duly considered, since arbitrarily chosen source distributions would merely produce profile forms the ultimate shape of which it would be impossible to foresee. The only essential thing will be to so modify the form of a Kármán-Trefftz profile that the nose is given a fuller form, the location of the maximum profile thickness is changed, or a different mean-line form is prescribed; this means the application of the source distributions leading to the Joukowski profile (fig. 33a) and to the crescent (fig. 33c) with edge angle δ and superposition by the simplest possible additive distributions $f_z\left(\frac{\xi}{a'}\right)$ with a flow function $Q_z\left(\frac{x}{a'}; \frac{\bar{y}}{a'}\right)$. Then the stream function of a symmetrical profile for the flow in x-axis direction is given by:

$$\frac{\Psi_x}{a' V_x} = \frac{y}{a'} + \frac{d}{a} Q_1\left(\frac{x}{a}; \frac{\bar{y}}{a'}\right)$$

$$+ \frac{1}{2} \delta \overline{Q}_5\left(\frac{x}{a'}; \frac{\bar{y}}{a'}\right) + \frac{h}{a'} Q_z\left(\frac{x}{a'}; \frac{\bar{y}}{a'}\right) \qquad (98)$$

where $\frac{h}{a'}$ is a constant. The type of additive distribution $f_z\left(\frac{\xi}{a'}\right)$ depends upon the desired profile shape. For a fuller nose, for example, a source and a sink of the same intensity is applied near the nose, or a doublet.

As to the displacement of the point of maximum profile thickness, on Joukowski profiles, it is about one-fourth aft of the leading edge; on Kármán-Trefftz profiles it moves with increasing edge angle δ closer toward the center. Suppose that a greater shift of maximum thickness toward profile center is desired. This displacement is favored by the function $f_4\left(\frac{\xi}{a'}\right)$ interpreted as source superposition (fig. 10), which heretofore appeared solely as quadratic small term and which by itself has a crescent (fig. 33b) with angle $\delta = 0$ as streamline. The maximum thickness occurs at $\frac{x}{a'}$, where the sources change to sinks. Selecting $f_z\left(\frac{\xi}{a'}\right) = f_4\left(\frac{\xi}{a'}\right)$, the total source distribution follows at

$$q\left(\frac{\xi}{a'}\right) \approx \frac{d}{a}\sqrt{\frac{1 - \xi/a'}{1 + \xi/a'}}\left(1 + 2\,\frac{\xi}{a'}\right) + \frac{1}{2}\,\delta\,\frac{\xi}{a'} + \frac{h}{a'}\,\frac{\xi}{a'}\sqrt{1 - \frac{\xi^2}{a'^2}}$$

where approximately $\left(\text{for } \frac{\xi}{a'} \ll 1\right) f_5\left(\frac{\xi}{a'}\right)$ for $\bar{f}_5\left(\frac{\xi}{a'}\right)$ (fig. 9). Putting $q\left(\frac{\xi}{a'}\right) = 0$, the point of maximum profile thickness $\frac{x_m}{a'}$ is:

$$\frac{h}{a'} = -\left[\frac{d}{a}\left(\frac{a'}{x_m} + \frac{1}{1 + \frac{x_m}{a'}}\right) + \frac{1}{2}\,\delta\,\frac{1}{\sqrt{1 - \frac{x_m^2}{a'^2}}}\right] \qquad (99)$$

Then the thickness is no longer computable from $\frac{d}{a}$ and δ, because $\frac{h}{a'}$ also exerts no effect upon it. Therefore, the thickness is prescribed at a selected point $\frac{x}{a'}$

so that $\frac{D}{a'} = 2\frac{\bar{y}}{a'}$. The streamline representing a symmetrical profile — curved profiles being discounted — must therefore pass through the point with the coordinates $\frac{x_1}{a'}$ and $\frac{1}{2}\frac{D}{a'}$, and carry the identification $\frac{\psi_x}{a' V_x} = 0$. Therewith equation (98) becomes

$$\frac{1}{2}\frac{D}{a'} = \frac{d}{a} Q_1\left(\frac{x_1}{a'}; \frac{1}{2}\frac{D}{a'}\right) + \frac{1}{2}\delta \bar{Q}_5\left(\frac{x_1}{a'}; \frac{1}{2}\frac{D}{a'}\right) + \frac{h}{a'} Q_4\left(\frac{x_1}{a'}\frac{1}{2}\frac{D}{a'}\right) \qquad (100)$$

Besides the thickness $\frac{D}{a'}$ at $\frac{x_1}{a'}$ the point of maximum thickness $\frac{x_m}{a'}$ and the edge angle δ are given. The values of $Q_\nu\left(\frac{x_1}{a'}; \frac{1}{2}\frac{D}{a'}\right)$ being obtainable from figures 15, 16, and 20, the two constants $\frac{d}{a}$ and $\frac{h}{a'}$ themselves follow from equations (99) and (100). The result, for cambered profiles, to which the known vortex distributions are applied, is the flow function

$$\frac{\psi_x}{a' V_x} = \frac{\bar{y}}{a'} + \frac{y_s}{a'} + \frac{d}{a} Q_1\left(\frac{x}{a'}; \frac{\bar{y}}{a'}\right) + \frac{1}{2}\delta \bar{Q}_5\left(\frac{x}{a'}; \frac{\bar{y}}{a'}\right) + \frac{h}{a'} Q_4\left(\frac{x}{a'}; \frac{\bar{y}}{a'}\right) + 2 \tan \beta_1 \left[W_3\left(\frac{x}{a'}; \frac{\bar{y}}{a'}\right) - W_3(1;0)\right] - \frac{\mu_1}{4}\left\{\left[W_2\left(\frac{x}{a'}; \frac{\bar{y}}{a'}\right) - W_2(1;0)\right] + 6\left[W_4\left(\frac{x}{a'}; \frac{\bar{y}}{a'}\right) - W_4(1;0)\right]\right\} \qquad (101)$$

where, according to equation (53), the ordinate $\frac{y_s}{a'}$ of the plane of the singularities is given by

$$\frac{y_s}{a'} = \left(\tan \beta_1 - \frac{\mu_1}{2}\frac{x}{a'}\right)\left(1 - \frac{x^2}{a'^2}\right) \qquad (102)$$

Since only linear terms are involved, $\tan \beta_1$ and μ_1 no longer afford an accurate form of the median line of the profile (the form of the mean line remains for disappearing thickness only) as is readily seen on the first approximation in figure 21 (third profile). However, the camber of this median line can be established by prescribing a point $P\left(\frac{x}{a'};\frac{\bar{y}}{a'} > 0\right)$ as profile point and computing $\tan \beta_1$ for this point from equation (101); whereas μ_1 is defined from the desired 0 angle of attack $\alpha^\circ = -\left(\beta_1 - \frac{\mu_1}{4}\right)$. It is best to select the point with the abscissa $\frac{x}{a'} = 0$ and the ordinate $\frac{\bar{y}}{a'} = \tan \beta + \frac{1}{2}\frac{D_o}{a'} = \frac{y_s}{a'} + \frac{\bar{y}}{a'}$, where $\frac{D_o}{a'}$ can be given according to equation (100) or computed for a symmetrical profile by means of equation (98); $\tan \beta$ is the desired profile camber $\tan \beta \leqq \tan \beta_1$.

To illustrate: Take $\tan \beta_1 = 0.08$, $\mu_1 = 0.038$ and $\delta = 16^\circ$ from the NACA 4418 airfoil section and shift the position of the maximum thickness toward point $\frac{x}{a'} = -0.2$; while $\frac{D_o}{a'} = 0.32$ remains for $\frac{x}{a'} = 0$. Then, according to (99) and (100), $\frac{d}{a} = 0.096$ and $\frac{h}{a'} = 0.068$. Next is computed the value of the flow function $\frac{\Psi_x}{a' V_x}$ from (101) and (102) for different abscissas $\frac{x}{a'}$ and several ordinates $\frac{\bar{y}}{a'} = 0.0, 0.05, 0.1, 0.15$, by posting the values $Q_\nu\left(\frac{x}{a'};\frac{\bar{y}}{a'}\right)$ and $W_\nu\left(\frac{x}{a'};\frac{y}{a'}\right)$ from the figures 15 to 20 or tables 1 to 7 and plotting the flow function against

$$\frac{y}{a'} = \frac{\bar{y}}{a'} + \frac{y_s}{a'}$$

in figure 34. The values $\frac{y}{a'}$ for $\frac{\Psi_x}{a' V_x} = 0$ are the points of the streamline $\frac{\Psi_x}{a' V_x} = 0$ of the looked-for profile. (The method of computing a profile from the singularities corresponds to that by Fuhrmann (reference 6) and can be used for any arrangement of singularities.) For the example in question the profile of figure 35 is obtained. The nose is scarcely changed by the distribution $f_4\left(\frac{\xi}{a'}\right)$; it remains the same as on the Karman-Trefftz profile, whence its curvature circle is given with sufficient accuracy by equation (15) according to reference (3). The foremost profile point is by $\frac{1}{2}\frac{\rho}{a'}$ from point $A_2'\left(\frac{x}{a'} = -1.0\right)$. The profile presents a substantially different thickness curve from a normal Kármán-Trefftz profile and resembles those developed by Piercy, Piper, and Preston (reference 9) by conformal transformation.

According to previous considerations, equation (59) can be retained for the flow along the y axis. The speeds $\frac{u}{V_\infty}$ and $\frac{v}{V_\infty}$ are lastly obtained by differentiation of (98), (101), and (59). The individual portions can be read off from figures 24 to 28. Since, in this instance, the profile form has been defined from the singularity distributions, the pressure distribution itself can be computed for these profiles also. Admittedly, a close approximation is obtained only for small α, since the streamline Ψ_y is usually not exactly fulfilled.

Translation by J. Vanier,
National Advisory Committee
for Aeronautics.

REFERENCES

1. Birnbaum, W.: Die trägende Wirbelflache als Hilfsmittel zur Behandlung des ebenen Problems der Tragflügeltheorie. Z.f.a.M.M., Bd, 3, Heft 4, Aug. 1923, pp. 290-97.

2. Glauert, H.: A Theory of Thin Aerofoils. R. & M. No. 910, British A.R.C., 1924.

3. Betz, A., and Keune, F.: Verallgemeinerte Karman-Trefftz-Profile. Luftfahrtforschung, Bd, 13, Nr. 10, Oct. 12, 1936, pp. 336-45; Jahrb. der Luftfahrtforschung 1937, pp. I 38-I 47.

4. von Kármán, Th.: Calculation of Pressure Distribution on Airship Hulls. T.M. No. 574, NACA 1930.

5. Lotz, I.: Calculation of Potential Flow Past Airship bodies in Yaw. T.M. No. 675, NACA, 1932.

6. Fuhrmann, G.: Theoretische und experimentelle Untersuchungen an Ballonmodellen. Jahrb. der Motorluftschiff-Studiengesellschaft, 1911-12, pp. 65-123.

7. Jacobs, Eastman N., Ward, Kenneth E., and Pinkerton, Robert M.: The Characteristics of 78 Related Airfoil Sections from Tests in the Variable-Density Wind Tunnel. Rep. No. 460, NACA, 1933.

8. Ergebnisse der Aerodynamischen Versuchsanstalt zu Göttingen. Lfg. IV, 1932, Verlag R. Oldenbourg. (München).

9. Piercy, N. A. V., Piper, R. W., and Preston, J. H.: A New Family of Wing Profiles. Phil. Mag., vol. 24, 1937, pp. 425-44, and 1126.

TABULATION

$$\frac{u}{V_\infty} = \cos\alpha\left[\frac{\partial\frac{\Psi_x}{a'V_\infty}}{\partial\, y/a'} + \frac{\partial\frac{\Psi_y}{a'V_\infty}}{\partial\, y/a'}\operatorname{tg}\alpha\right]$$

	Sign	$\frac{\partial Q_1\left(\frac{x}{a'};\frac{\bar{y}}{a'}\right)}{\partial\, y/a'}$	$\frac{\partial \bar{Q}_3\left(\frac{x}{a'};\frac{\bar{y}}{a'}\right)}{\partial\, y/a'}$	$\frac{\partial W_3\left(\frac{x}{a'};\frac{\bar{y}}{a'}\right)}{\partial\, y/a'}$	$\frac{\partial W_2\left(\frac{x}{a'};\frac{\bar{y}}{a'}\right)}{\partial\, y/a'}$	$\frac{\partial W_4\left(\frac{x}{a'};\frac{\bar{y}}{a'}\right)}{\partial\, y/a'}$	Quadratic term
$\frac{\partial\frac{\Psi_x}{a'V_\infty}}{\partial\, y/a'} =$	$+1$	$+\frac{d}{a}$	$+\frac{1}{2}\delta$	$-\frac{1}{4}\mu$	$+2\operatorname{tg}\beta$	$-\frac{3}{2}\mu$	$+\frac{\partial g_x}{\partial\, y/a'}$
$\frac{\partial\frac{\Psi_y}{a'V_\infty}}{\partial\, y/a'} =$				$+\left(1+2\frac{d}{a}+\varkappa\right)$	$-2\frac{d}{a}$		$-\frac{\partial g_y}{\partial\, y/a'}$

$$\frac{v}{V_\infty} = -\cos\alpha\left[\frac{\partial\frac{\Psi_x}{a'V_\infty}}{\partial\, x/a'} - \frac{\partial\frac{\Psi_y}{a'V_\infty}}{\partial\, x/a'}\operatorname{tg}\alpha\right]$$

	Sign	$\frac{\partial Q_1\left(\frac{x}{a'};\frac{\bar{y}}{a'}\right)}{\partial\, x/a'}$	$\frac{\partial \bar{Q}_3\left(\frac{x}{a'};\frac{\bar{y}}{a'}\right)}{\partial\, x/a'}$	$\frac{\partial W_3\left(\frac{x}{a'};\frac{\bar{y}}{a'}\right)}{\partial\, x/a'}$	$\frac{\partial W_2\left(\frac{x}{a'};\frac{\bar{y}}{a'}\right)}{\partial\, x/a'}$	$\frac{\partial W_4\left(\frac{x}{a'};\frac{\bar{y}}{a'}\right)}{\partial\, x/a'}$	Quadratic term
$\frac{\partial\frac{\Psi_x}{a'V_\infty}}{\partial\, x/a'} =$		$+\frac{d}{a}$	$+\frac{1}{2}\delta$	$-\frac{1}{4}\mu$	$+2\operatorname{tg}\beta$	$-\frac{3}{2}\mu$	$+\frac{\partial g_x}{\partial\, x/a'}$
$\frac{\partial\frac{\Psi_y}{a'V_\infty}}{\partial\, x/a'} =$	$+1$			$-\left(1+2\frac{d}{a}+\varkappa\right)$	$+2\frac{d}{a}$		$-\frac{\partial g_y}{\partial\, x/a'}$

	$\frac{\partial Q_1\left(\frac{x}{a'};\frac{\bar{y}}{a'}\right)}{\partial\, x/a'}$	$\frac{\partial \bar{Q}_3\left(\frac{x}{a'};\frac{\bar{y}}{a'}\right)}{\partial\, x/a'}$	$\frac{\partial W_3\left(\frac{x}{a'};\frac{\bar{y}}{a'}\right)}{\partial\, x/a'}$	$\frac{\partial W_2\left(\frac{x}{a'};\frac{\bar{y}}{a'}\right)}{\partial\, x/a'}$	$\frac{\partial W_4\left(\frac{x}{a'};\frac{\bar{y}}{a'}\right)}{\partial\, x/a'}$	$\frac{\partial Q_4\left(\frac{x}{a'};\frac{\bar{y}}{a'}\right)}{\partial\, x/a'}$
$\frac{\partial g_x}{\partial\, x/a'}$	$+\frac{d}{a}\left(2\frac{d}{a}+\varkappa\right)$	$+\frac{3}{4}\varkappa\delta$	$-\frac{d}{a}\operatorname{tg}\beta$	$+2\operatorname{tg}\beta\left(2\frac{d}{a}+\varkappa\right)$	$-6\frac{d}{a}\operatorname{tg}\beta$	$-6\frac{d^2}{a^2}$

$$\frac{\partial Q_4}{x/a'} = +\frac{\partial W_4}{d\, y/a'} \text{ (Equation 85).}$$

Table 1. Flow function $Q_1\left(\frac{x}{a'};\frac{\bar{y}}{a'}\right)$ of the source distribution $f_1(\xi/a')$ of the Joukowski Profile.

$\frac{x}{a'}$ \ $\frac{\bar{y}}{a'}$	0	0,05	0,1	0,15	0,2	0,3
+ 0,75	—0,191	—0,210	—0,221	—0,231	—0,242	— 0,264
+ 0,50	—0,450	—0,449	—0,448	—0,446	—0,444	— 0,417
+ 0,25	—0,718	—0,698	—0,672	—0,652	—0,640	— 0,605
0	—1,028	—0,970	—0,914	—0,868	—0,834	— 0,764
— 0,25	—1,220	—1,148	—1,083	—1,026	—0,965	— 0,860
— 0,50	—1,328	—1,223	—1,138	—1,061	—0,991	— 0,853
— 0,75	—1,162	—1,050	—0,964	—0,892	—0,824	— 0,729
— 1,00	0	—0,318	—0,376	—0,403	—0,414	— 0,439

Table 2. Flow function $\bar{Q}_5\left(\frac{x}{a'};\frac{\bar{y}}{a'}\right)$ of the source distribution $\bar{f}_5(\xi/a')$ of the crescent

$\frac{x}{a'}$ \ $\frac{\bar{y}}{a'}$	0	0,05	0,1	0,15	0,2	0,3
0	—0,477	—0,442	—0,420	—0,401	—0,385	— 0,334
± 0,25	—0,449	—0,405	—0,383	—0,369	—0,350	— 0,312
± 0,50	—0,352	—0,324	—0,304	—0,289	—0,279	— 0,253
± 0,75	—0,195	—0,195	—0,190	—0,185	—0,177	— 0,177
± 1,00	0	—0,036	—0,055	—0,069	—0,080	— 0,098

Table 3. Flow function $W_2\left(\frac{x}{a'};\frac{\bar{y}}{a'}\right)$ of the vortex distribution $f_2(\xi/a')$ of the flat plate.

$\frac{x}{a'}$ \ $\frac{\bar{y}}{a'}$	0	0,05	0,1	0,15	0,2	0,3
+ 0,75	+ 0,75	+0,78	+0,80	+0,82	+0,84	+ 0,87
+ 0,50	+ 0,50	+0,53	+0,566	+0,595	+0,626	+ 0,68
+ 0,25	+ 0,25	+0,280	+0,319	+0,364	+0,407	+ 0,483
0	0	+0,05	+0,100	+0,149	+0,200	+ 0,30
— 0,25	— 0,25	—0,195	—0,134	—0,064	0	+ 0,127
— 0,50	— 0,50	—0,419	—0,338	—0,250	—0,160	— 0,003
— 0,75	— 0,75	—0,628	—0,509	—0,385	—0,270	— 0,065
— 1,00	— 1,00	—0,570	—0,396	—0,254	—0,136	+ 0,062

Table 4. Flow function $W_3\left(\frac{x}{a'};\frac{\bar{y}}{a'}\right)$ of the vortex distribution $f_3(\xi/a')$ of the curved plate.

$\frac{x}{a'}$ \ $\frac{\bar{y}}{a'}$	0	0,05	0,1	0,15	0,2	0,3
0	—0,250	—0,203	—0,158	—0,114	—0,070	+ 0,010
± 0,25	—0,220	—0,175	—0,126	—0,089	—0,048	+ 0,032
± 0,50	—0,125	—0,085	—0,045	—0,008	+0,028	+ 0,095
± 0,75	+0,033	+0,064	+0,092	+0,120	+0,147	+ 0,196
± 1,00	+0,25	+0,255	+0,265	+0,275	+0,288	+ 0,315

Table 5. Flow function $W_4\left(\frac{x}{a'};\frac{\bar{y}}{a'}\right)$ of the vortex distribution $f_4(\xi/a')$ of the S-shaped mean line.

$\frac{x}{a'}$ \ $\frac{\bar{y}}{a'}$	0	0,05	0,1	0,15	0,2	0,3
0	0	0	0	0	0	0
± 0,25	∓ 0,127	∓ 0,118	∓ 0,108	∓ 0,098	∓ 0,089	∓ 0,068
± 0,50	∓ 0,212	∓ 0,192	∓ 0,174	∓ 0,159	∓ 0,145	∓ 0,119
± 0,75	∓ 0,238	∓ 0,216	∓ 0,197	∓ 0,179	∓ 0,164	∓ 0,139
± 1,00	∓ 0,165	∓ 0,164	∓ 0,157	∓ 0,148	∓ 0,142	∓ 0,129

Table 6. Flow function $Q_4\left(\frac{x}{a'};\frac{\bar{y}}{a'}\right)$ of the source distribution $f_4(\xi/a')$ (Figure 33).

$\frac{x}{a'}$ \ $\frac{\bar{y}}{a'}$	0	0,05	0,1	0,15	0,2	0,3
0	—0,339	—0,316	—0,298	—0,277	—0,259	— 0,231
± 0,25	—0,309	—0,291	—0,274	—0,256	—0,239	— 0,213
± 0,50	—0,218	—0,207	—0,199	—0,189	—0,180	— 0,164
± 0,75	—0,10	—0,100	—0,102	—0,106	—0,108	— 0,109
± 1,0	0	—0,018	—0,030	—0,042	—0,051	— 0,060

Table 7. Additive values to the flow function

$\frac{\bar{y}}{a'}$ \ $\frac{x}{a'}$	$Q_1\left(\frac{x}{a'},\frac{\bar{y}}{a'}\right)$ —0,95	—1,05	—1,10	$Q_4\left(\frac{x}{a'};\frac{\bar{y}}{a'}\right)$ —0,95	—1,05	—1,10
0	—0,582	0	0	—0,009	0	0
0,025	—0,559	—0,100	—0,047	—0,020	—0,007	—0,004
0,050	—0,531	—0,170	—0,107	—0,028	—0,0145	—0,012
0,10	—0,500	—0,258	—0,204	— ,042	—0,0233	—0,022

$\frac{\bar{y}}{a'}$ \ $\frac{x}{a'}$	$\bar{Q}_5\left(\frac{x}{a'},\frac{\bar{y}}{a'}\right)$ —0,95	—1,05	—1,10	$W_2\left(\frac{x}{a'};\frac{\bar{y}}{a'}\right)$ —0,95	—1,05	—1,10
0	— 0,039	0	0	— 0,95	—0,424	— 0,184
0,025	— 0,040	—0,016	—0,009	— 0,82	—0,374	— 0,170
0,050	— 0,054	—0,026	—0,019	— 0,68	—0,329	— 0,154
0,10	— 0,080	—0,045	—0,037	— 0,47	—0,241	— 0,102

$W_3\left(\frac{x}{a'};\frac{\bar{y}}{a'}\right)$ —0,95	—1,05	1,10	$W_4\left(\frac{x}{a'};\frac{\bar{y}}{a'}\right)$ —0,95	—1,05	—1,10
+ 0,205	+ 0,290	+ 0,334	+ 0,195	+ 0,157	+ 0,139
+ 0,209	+ 0,290	+ 0,330	+ 0,182	+ 0,151	+ 0,138
+ 0,217	+ 0,292	+ 0,327	+ 0,176	+ 0,148	+ 0,135
+ 0,232	+ 0,301	+ 0,327	+ 0,171	+ 0,142	+ 0,131

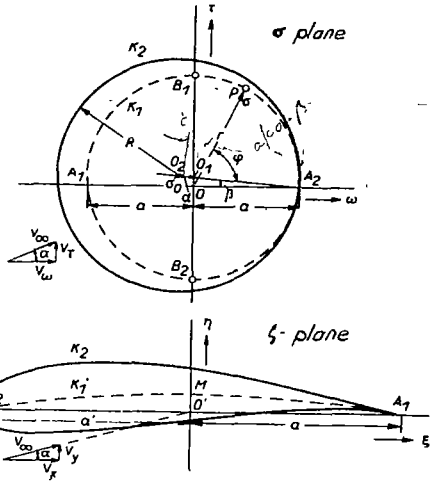

Figure 1.-Circle transformed on a curved Joukowsky-profile.

ξ/a	$\frac{1}{\kappa}\epsilon(\xi/a)$
± 098	± 0055
± 0975	± 0060
± 095	± 0070
± 090	± 0085
± 075	± 0090
± 050	± 0080
± 025	± 0045
0	0

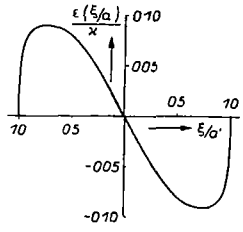

Figure 5.-The additive formation $\frac{1}{\kappa}\epsilon\left(\frac{\xi}{a'}\right)$

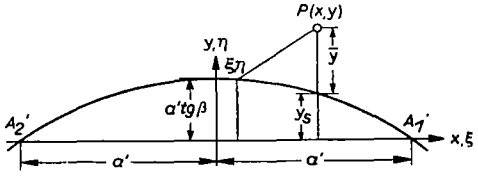

Figure 8.-Simplification of integral of flow function.

ξ/a	$\bar{f}_5(\xi/a')$
± 10	± 0
± 095	± 0800
± 090	± 0792
± 075	± 0717
± 050	± 0506
± 025	± 0261
± 00	0

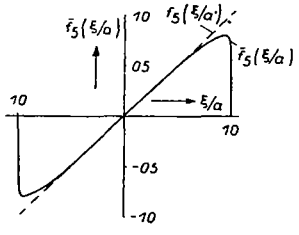

Figure 9.-Source distribution $\bar{f}_5\left(\frac{\xi}{a'}\right)$ of crescent for edge angle δ=1.0

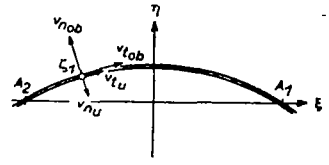

Figure 2.-Velocity jump at profile mean line.

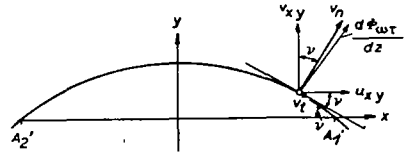

Figure 3.-Division of speed on mean line in normal and tangential components.

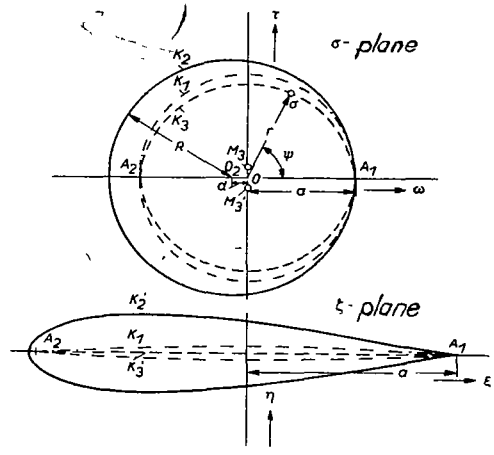

Figure 4.-Mapping of a circle on a symmetrical Kármán-Treffts profile.

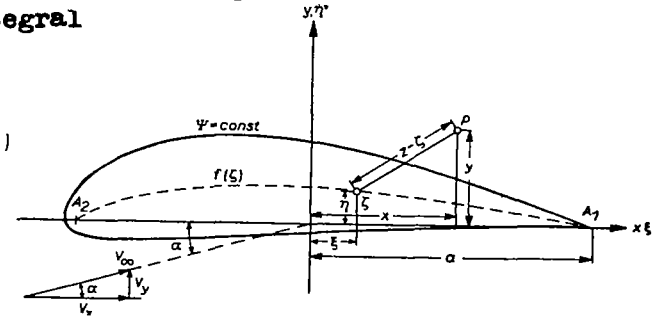

Figure 7.-Identification of complex flow potential in the plane of the section.

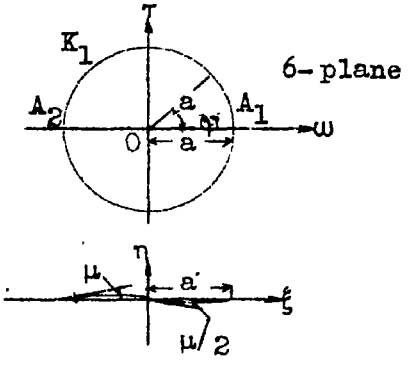

Figure 6.- Circle mapped on S-shaped mean line.

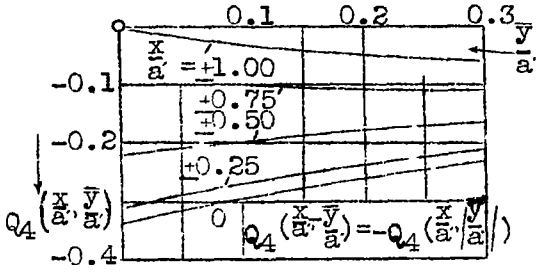

Figure 20.- Flow function $Q_4\left(\frac{x}{a'}, \frac{y}{a'}\right)$ of the additive source distribution $f_4\left(\frac{\xi}{a'}\right)$.

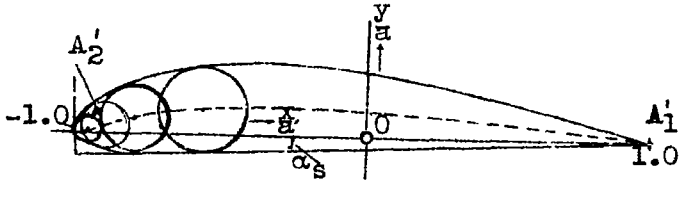

Figure 29.- Gottinger airfoil section No. 624.

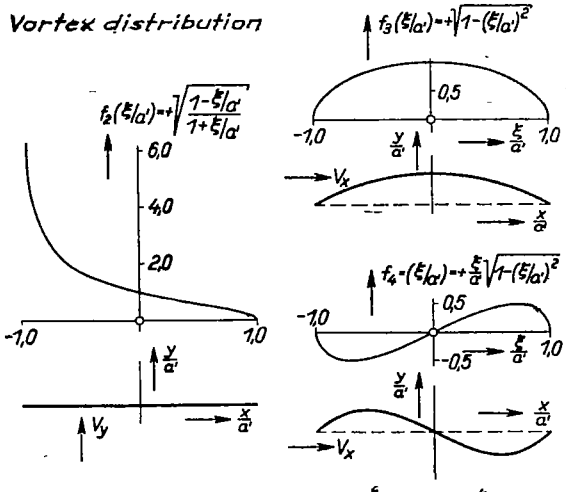

Figure 10.-Functions $f_2(\frac{\xi}{a'})$ $f_3(\frac{\xi}{a'})$ and $f_4(\frac{\xi}{a'})$ for the superposed vortex distribution density and related forms of mean lines.

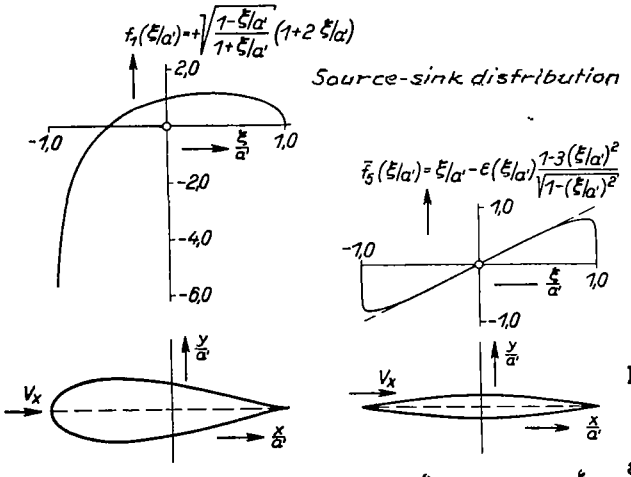

Figure 11.-Functions $f_1(\frac{\xi}{a'})$ and $f_5(\frac{\xi}{a'})$ for the superposed source distribution density and related contours.

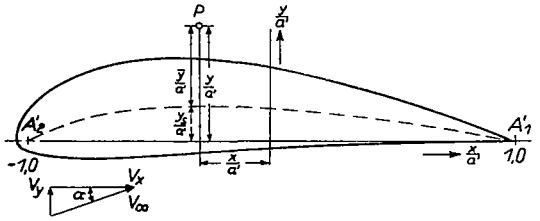

Figure 12.-Decomposition of y ordinate in plane of section.

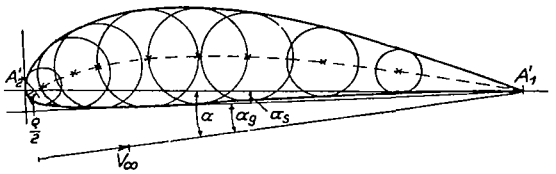

Figure 13.-Identification of mean line and axis $A'_1A'_2$ of a Kármán-Treffts profile.

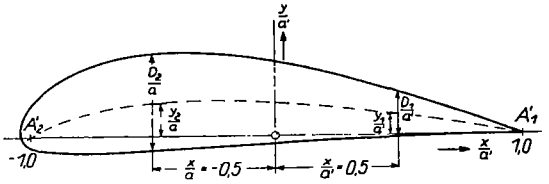

Figure 14.-Solution of the four profile constants of a generalized Kármán-Treffts profile.

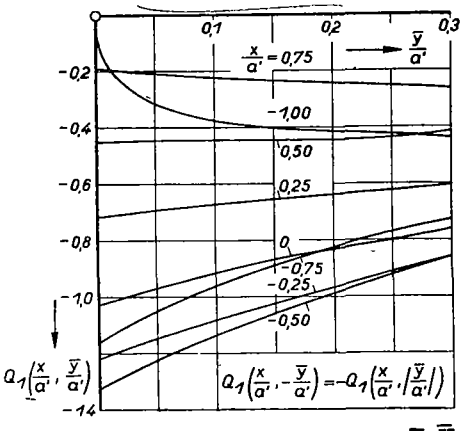

Figure 15.-Flow function $Q_1(\frac{x}{a'},\frac{\bar{y}}{a'})$ of source distribution $f_1(\frac{\xi}{a'})$ of the Joukowski profile plotted against ordinate $\frac{\bar{y}}{a'}$ for the different abscissas $\frac{x}{a'}$.

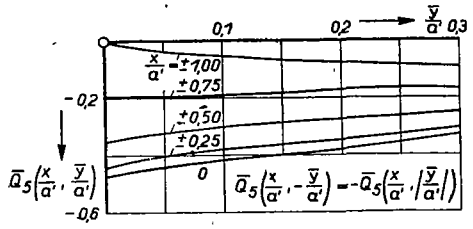

Figure 16.-Flow function $\bar{Q}_5(\frac{x}{a'},\frac{\bar{y}}{a'})$ of source distribution $f_5(\frac{\xi}{a'})$ of the crescent.

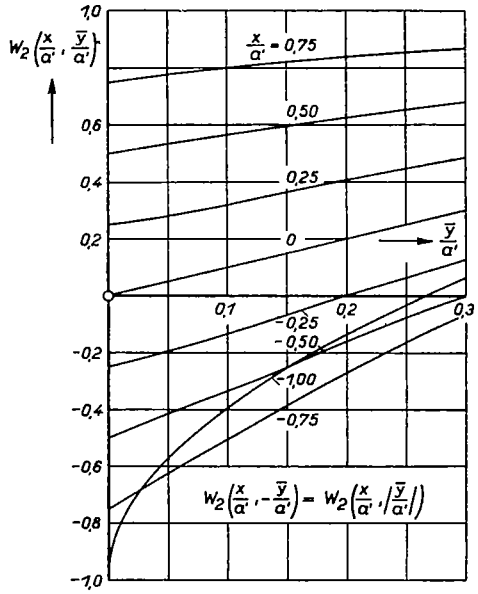

Figure 17.-Flow function $W_2\left(\frac{x}{a'};\frac{y}{a'}\right)$ of vortex distribution $f_2\left(\frac{\xi}{a'}\right)$ of the flat plate plotted against $\frac{y}{a'}$ for different $\frac{x}{a'}$ (W_2 [1;0]=+1,00).

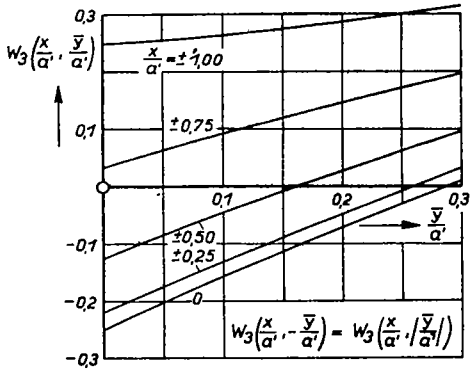

Figure 18.-Flow function $W_3\left(\frac{x}{a'};\frac{y}{a'}\right)$ of vortex distribution $f_3\left(\frac{\xi}{a'}\right)$ of the curved plate plotted against $\frac{y}{a'}$ for different $\frac{x}{a'}$.

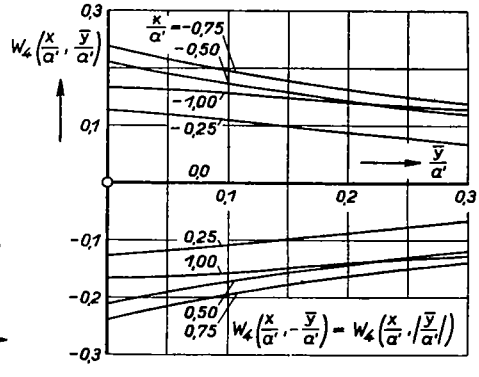

Figure 19.-Flow function $W_4\left(\frac{x}{a'};\frac{y}{a'}\right)$ of vortex distribution $f_4\left(\frac{\xi}{a'}\right)$ of the S-shaped mean plotted against $\frac{y}{a'}$ for different $\frac{x}{a'}$. →

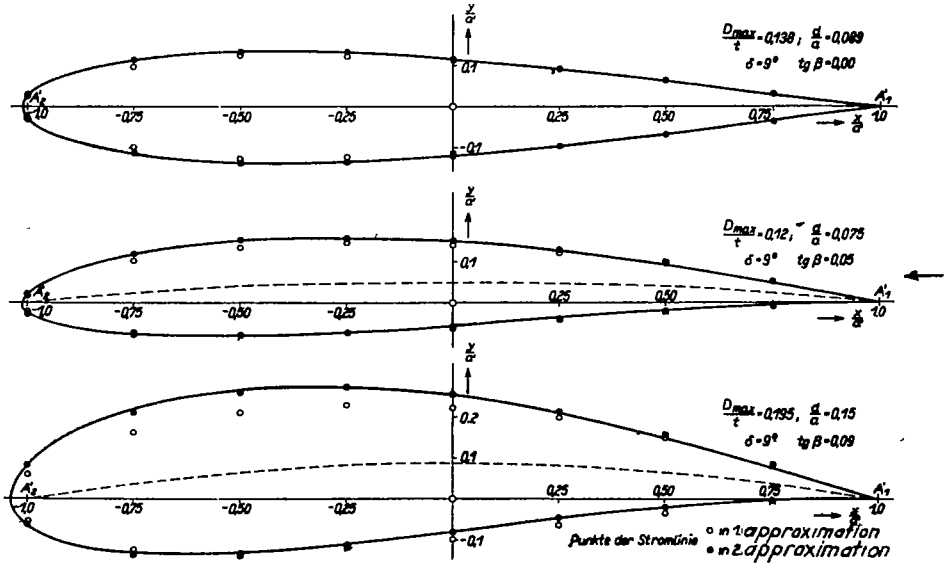

Figure 21.-Example;approximation of three Karman-Treffts profiles by the singularity distribution method.

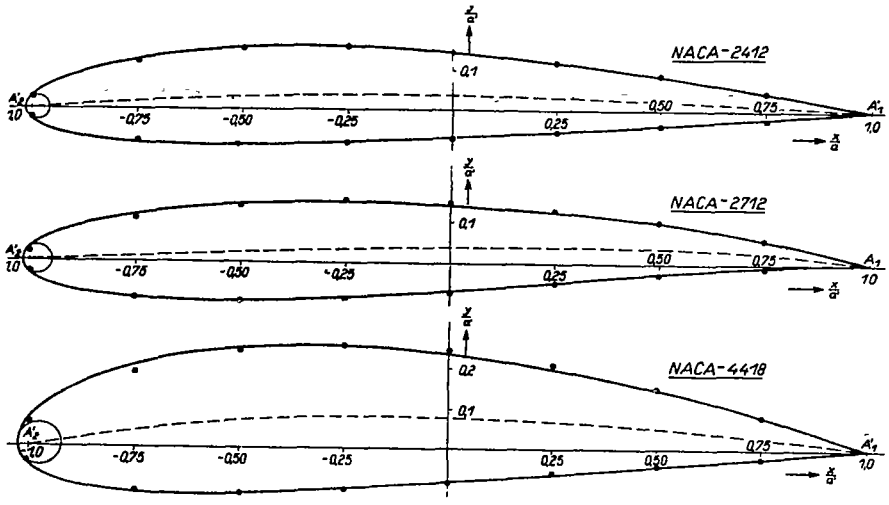

Figure 22.-Example; approximation of three NACA airfoil sections.

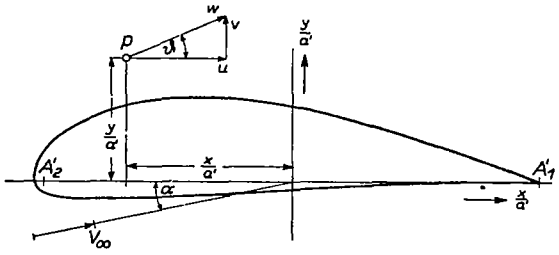

Figure 23.-Speed in vicinity of a profile.

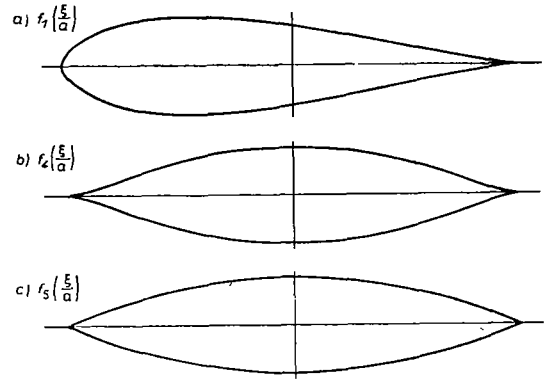

Figure 33.-Profile forms obtained by the individual source distributions in parallel flow along x axis.

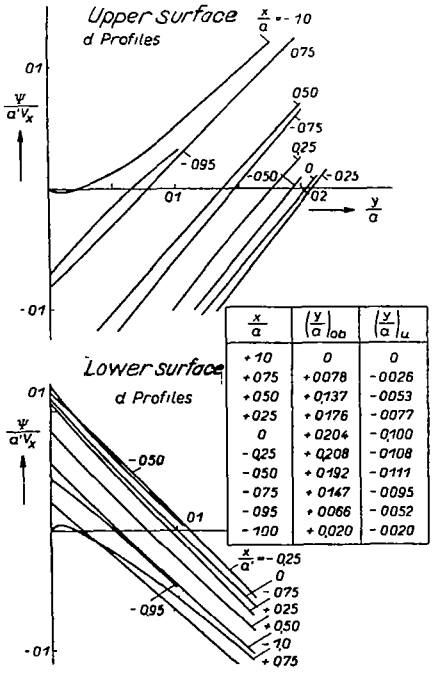

$\frac{x}{a}$	$\left(\frac{v}{a}\right)_{ob}$	$\left(\frac{v}{a}\right)_{u}$
+10	0	0
+075	+0078	-0026
+050	+0137	-0053
+025	+0176	-0077
0	+0204	-0100
-025	+0208	-0108
-050	+0192	-0111
-075	+0147	-0095
-095	+0066	-0052
-100	+0020	-0020

Figure 34.-Example; the value of flow function $\frac{\psi_x}{aV_x}$ on individual points $\frac{x}{a'}$ for different ordinates $\frac{y}{a'}$ by given singularity distributions.

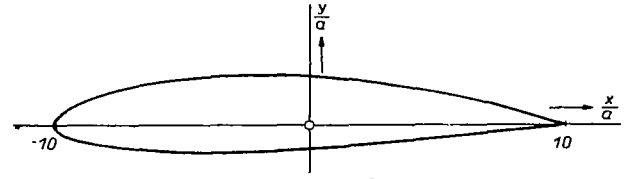

Figure 35.-New profile forms by prescribed special singularity distributions.

Figure 24.-Orthogonal system of velocities induced by the source distribution $f_1\left(\frac{\zeta}{a'}\right)$ of the Jowkowsky profile.

Figure 25.-Orthogonal system of velocities induced by the source distribution $f_5\left(\frac{\zeta}{a'}\right)$ of the crescent.

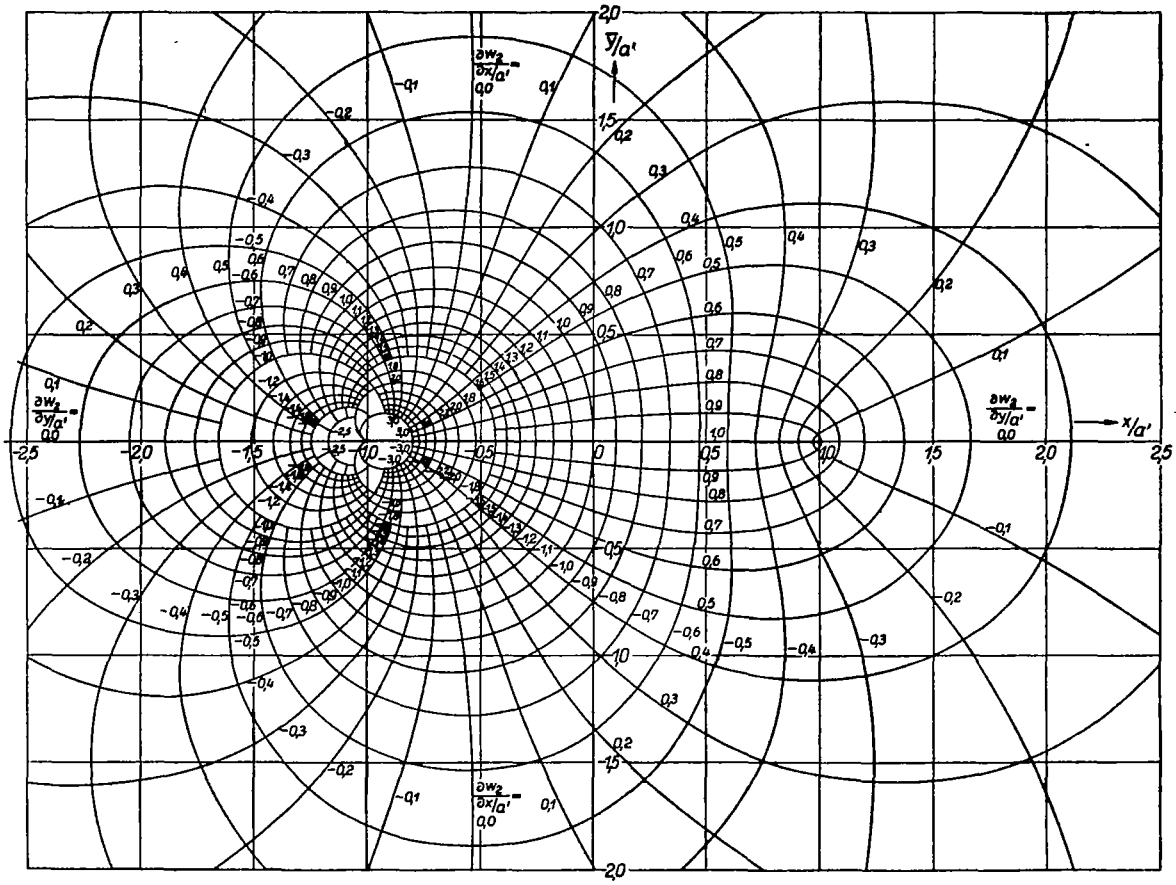

Figure 26.-Orthogonal system of velocities induced by the vortex distribution $f_2\left(\frac{\xi}{a'}\right)$ of the flat plate.

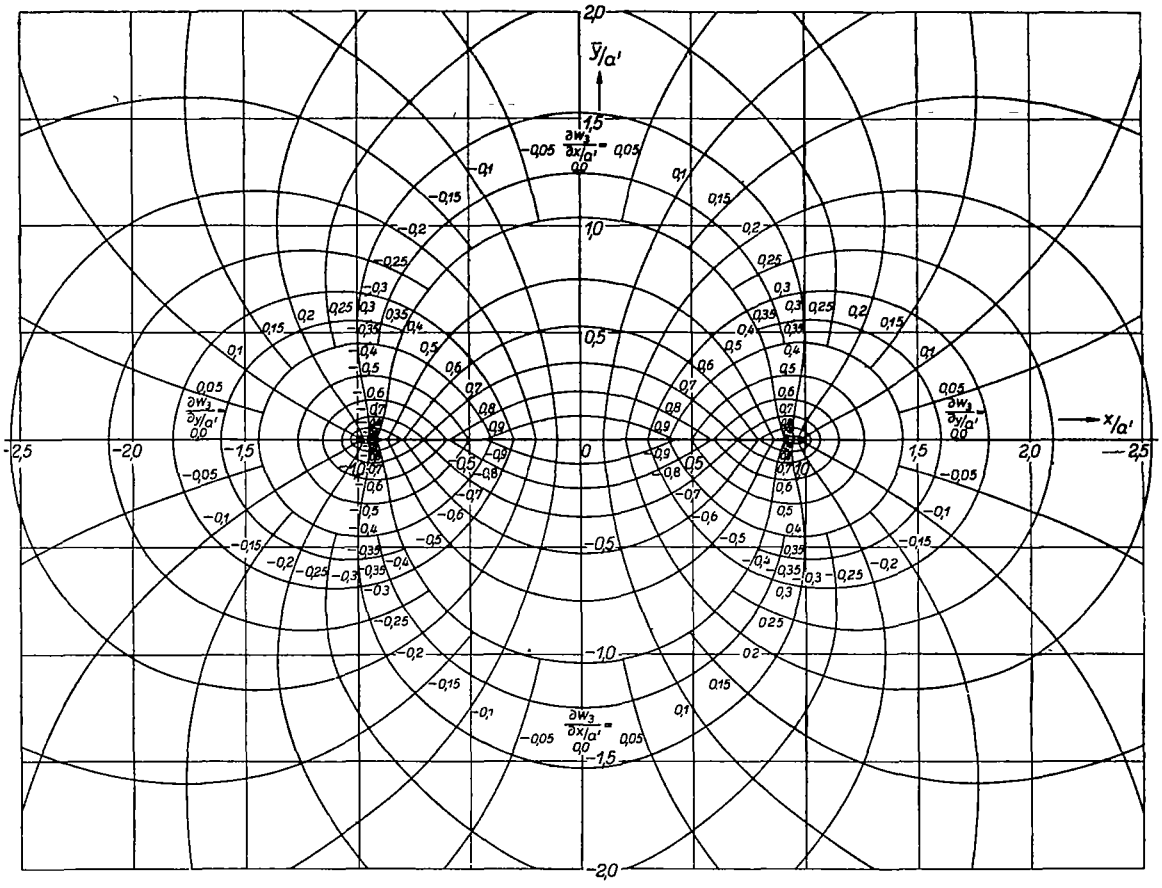

Figure 27.-Orthogonal system of speeds induced by curved plate vortex distribution $f_3\left(\frac{\xi}{a'}\right)$.

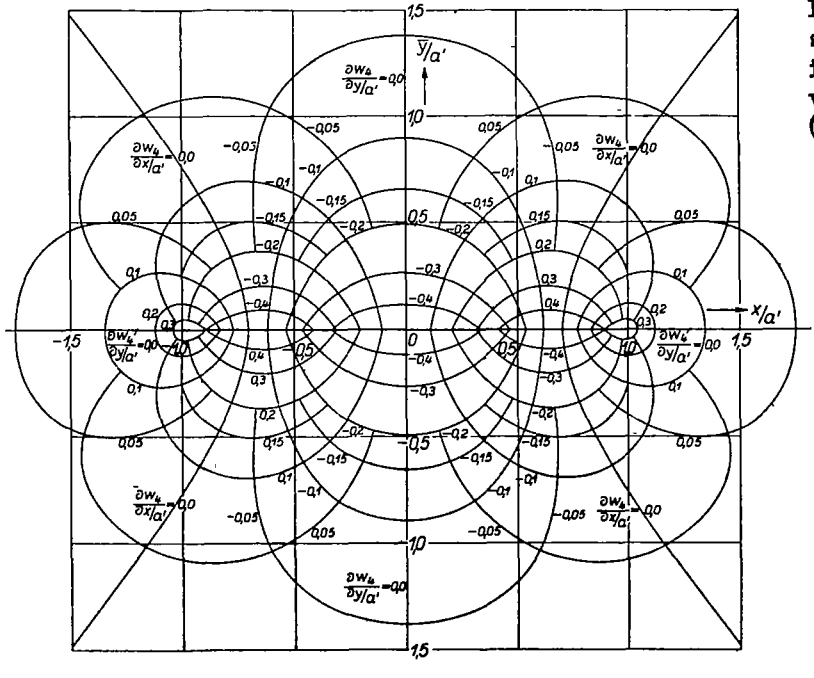

Figure 28.-Orthogonal system of speeds induced by vortex distribution $f_4\left(\frac{\xi}{a'}\right)$ of the S-shaped mean line.

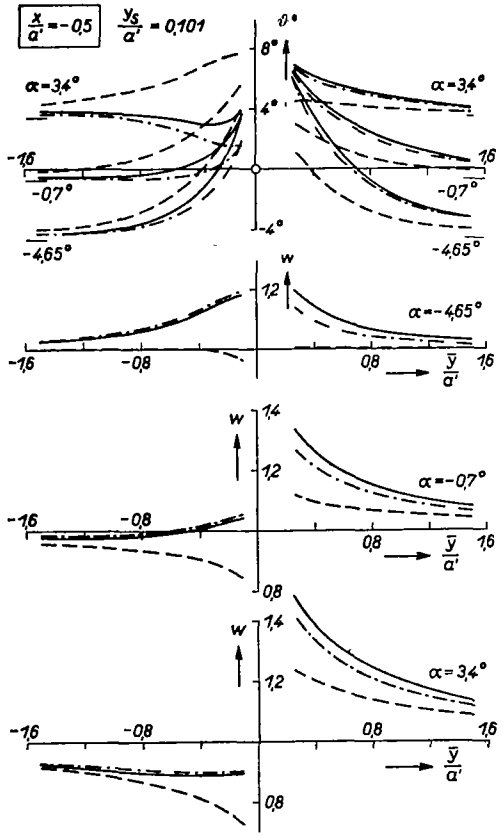

Figure 30.-Speeds in field of Göttinger airfoil section No.624; section $\frac{x}{a'} = -0,5$ parallel to y axis. Ommission of profile thickness affords the dashed curve, disregard of quadrative term $\frac{\partial f_x}{\partial x/a'}$ the dash-dot curve.

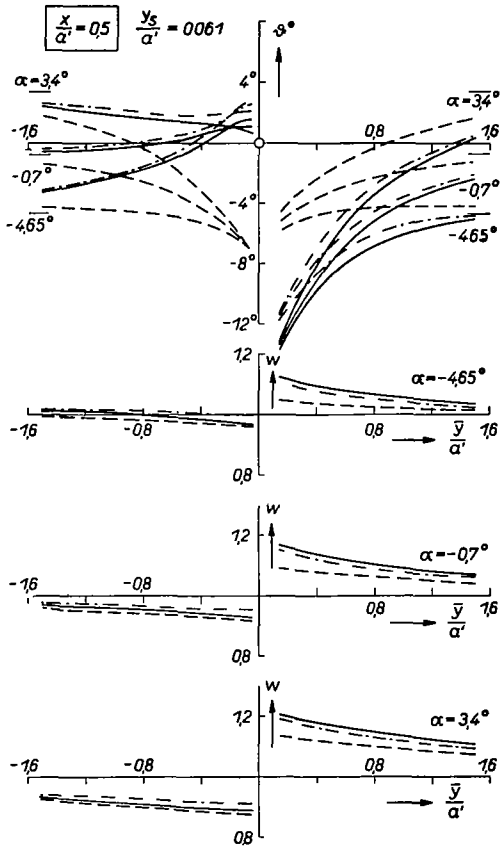

Figure 31.-Speeds in field of Göttinger airfoil section No.624; section $\frac{x}{a'} = +0,5$ parallel to y axis.

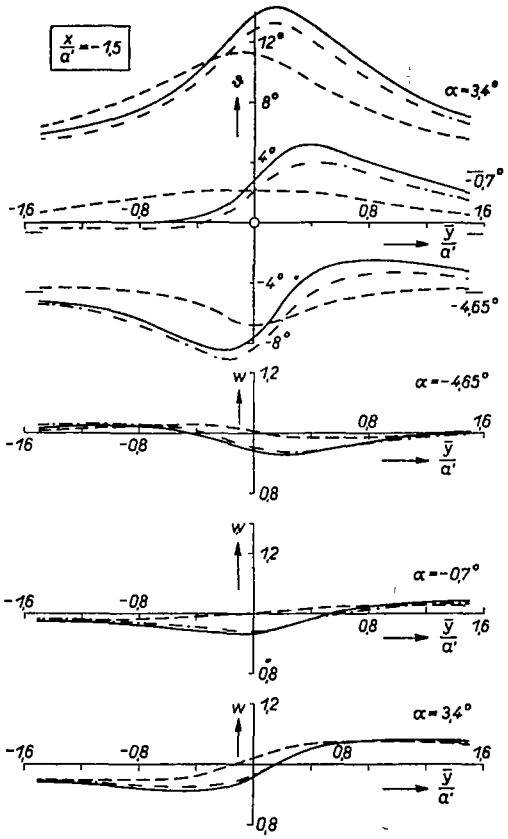

Figure 32.-Speeds in field of Göttinger airfoil section No.624; section $\frac{x}{a'} = -1,5$ parallel to y axis.